Faculdade de Engenharia da Universidade do Porto

Instituto de Investigação e Inovação em Saúde

Mechanomodulatory Hydrogel to Probe the Effect of Mechanical Cues on Fibroblast Response

Bruna Sofia Gonzaga de Nápoles

Master in Bioengineering

Supervisor: Prof. Dr. Rúben Filipe Brás Pereira, ICBAS/i3S, University of Porto
Co-supervisor: Dr. Flávia Raquel Teixeira de Castro, i3S, University of Porto

September 2022

This page was intentionally left blank.

Abstract

Impaired skin wound healing due to severe burn injury often leads to aberrant scar tissue formation as a result of excessive extracellular matrix (ECM) deposition and dysfunctional collagen turnover by fibroblast cells. However, despite extensive research on impaired wound healing and the advancement in skin tissue engineering, which have contributed to a significant decrease in burn-related mortality, they still present significant drawbacks such as excessive scar formation. The importance of mechanical forces in wound healing, scarring, and ECM remodeling has been highlighted, as a variety of cells involved in such biological processes are mechanosensitive, being able to perceive the surrounding mechanical forces and respond to them via several mechanisms. Thus, it is important to grasp how cells transduce the mechanical cues of the surrounding microenvironment at cellular and tissue level toward the development of strategies to promote wound healing. Innovative approaches based on the release of mechanotransduction inhibitors and mechanomodulatory devices are under investigation to overcome excessive scar formation and promote the formation of healthy skin.

This study investigated the effect of hydrogel mechanical properties on human dermal fibroblast behavior in three-dimension (3D). To recreate the key aspects of the ECM, a viscoelastic and dual-crosslinked hydrogel based on a pectin derivative polymer (PectX)[1] was designed and its properties were characterized in detail. To develop hydrogels with tunable mechanical properties, a dual crosslinking strategy using both physical (ionic) and chemical (Diels-Alder) crosslinking was employed. The PectX polymer had to be modified with either furan or maleimide groups, attaining a modification degree of 7.08 ± 0.29% and 8.51 ± 0.21%, respectively, to later promote the Diels-Alder reaction between them. The hydrogels were firstly biofunctionalized with a cell adhesive peptide (CGGGGRGDSP, cell-adhesive domain underlined) through Michael's addition reaction that provided biochemical cues for cell adhesion. Then, hydrogels were ionic crosslinked using calcium ions to adjust their rheology at 4°C, followed by a Diels-Alder reaction between maleimide and furan groups at 37°C. Through the variation of polymer concentration (2-4%) we were able to obtain elastic modulus values between 1528.31 ± 297.80 Pa and 3898.99 ± 486.31 Pa and viscous modulus values between 193.51 ± 73.30 Pa and 461.01 ± 111.76 Pa. By varying the calcium concentration (6-12 mM), it was possible to obtain hydrogels displaying elastic and viscous moduli from 921.40 ± 260.60 Pa to 1699.73 ± 50.03 Pa and 130.09 ± 42.07 to 230.08 ± 95.22 Pa, respectively. Cell behavior to these hydrogels demonstrated that the increase in calcium ions (Ca^{2+}) concentration led to an

[1] Disclosure: PectX is a derivative of pectin obtained by specific purification and chemical modification reactions. As a patent request is under preparation, the exact chemical composition and fabrication methods are confidential. Thus, in the scope of this dissertation, the polymer is referred to as PectX.

increase in cell adhesion and elongation, while the increase in polymer concentration had the opposite effect. Varying the concentration of the peptide also demonstrated that cell adhesion is enhanced as the peptide content increases, as expected. *De novo* fibronectin deposition, a major ECM component, was also evaluated at day 14, demonstrating that in both 2 and 3% hydrogels cells were able to form interconnecting cellular networks secreting large amounts of fibronectin, while in 4% hydrogels such behavior was hindered. In addition, multicellular fibroblast spheroids were produced to later be incorporated into the hydrogels. A greater contraction in the diameter of the spheroids was observable in the first 24 hours after seeding the molds, and their size continues to decrease during the 7-day culture period in the molds. The fibroblasts assembled in spheroids remained metabolically active throughout the 7-day experiment, though a decrease was observed that is directly related to the increase in cell density and spheroid size. Finally, the multicellular spheroids were embedded within the hydrogels to assess fibroblast migratory behavior. The results indicated that the increase in polymer concentration severely restricted the fibroblast's ability to migrate and invade the gel network. Furthermore, the maturation time of the spheroids did not have a highly significant impact on their migration and the cell density showed that although the spheroids with 2500 cells completely disassembled the spheroid, they were not sufficient to promote the formation of cellular interconnected networks, while the spheroids with 5000 and 10000 cells formed these structures.

Overall, we created a dual-crosslinked hydrogel with tunable mechanical properties through the combination of physical and chemical crosslinking strategies. Furthermore, we have demonstrated that the mechanical properties of such hydrogels play a regulatory role in key fibroblast functions such as proliferation, spreading, migration, and *de novo* ECM deposition.

Resumo

A cicatrização de feridas da pele, em particular de lesões graves provocadas por queimaduras, leva frequentemente à formação de tecido cicatricial anormal como resultado da deposição excessiva de componentes da matriz extracelular (MEC) e da conversão desregulada de colagénio realizada pelos fibroblastos. No entanto, apesar da extensiva investigação no âmbito da cicatrização de feridas e engenharia de tecidos da pele contribuir para a diminuição da mortalidade como resultado de queimaduras graves, ainda existem obstáculos significativos, tal como a formação excessiva de tecido de cicatrização. A importância das forças mecânicas na reparação de feridas, cicatrização e remodelação da MEC tem sido realçada em diversos estudos uma vez que as células envolvidas nestes processos biológicos são mecanosensíveis. Como tal, são capazes de percecionar as forças mecânicas circundantes e responder através de diversos mecanismos. Assim, é importante compreender de que forma as células percecionam os sinais mecânicos do microambiente circundante de forma a desenvolver estratégias mais eficazes para promover a cicatrização das feridas. Atualmente estão a ser investigadas abordagens inovadoras baseadas na libertação de inibidores de mechanotransdução e dispositivos mecanomoduladores para colmatar a formação excessiva de tecido de cicatriz e promover a formação de pele saudável.

Este estudo investigou o efeito das propriedades mecânicas do hidrogel no comportamento de fibroblastos humanos da derme em três dimensões. Para recriar aspetos chave da MEC, um hidrogel viscoelástico baseado num polímero derivado da pectina (PectX) foi desenvolvido e as suas propriedades foram caracterizadas em detalhe. Para desenvolver hidrogéis com propriedades mecânicas controláveis, foi utilizada uma estratégia de reticulação dupla envolvendo reações de reticulação física (iónica) e química (Diels-Alder). Inicialmente, o polímero (PectX) foi modificado com grupos furano e maleimidas para permitir a reação Diels-Alder, tendo-se obtido um grau de modificação de 7.08 ± 0.29% e 8.51 ± 0.21%, respetivamente. Os hidrogéis foram primeiramente biofuncionalizados com um péptido para promover a adesão celular (CGGGGRGDSP, domínio de adesão celular sublinhado) através da reação de adição de Michael. De seguida, os hidrogéis foram reticulados ionicamente utilizando iões de cálcio para ajustar a sua reologia a 4°C, seguido da reação Diels-Alder entre grupos maleimida e furano a 37°C. Através da variação da concentração de polímero (2-4%) foi possível obter valores do módulo elástico entre 1528.1 ± 297.80 Pa e 3898.99 ± 486.31 Pa e valores do módulo viscoso entre 193.51 ± 73.30 Pa e 461.01 ± 111.76 Pa. Variando a concentração de cálcio (6-12 mM), foi também possível obter hidrogéis com módulos elásticos e viscosos entre 921.40 ± 260.60 Pa a 1699.73 ± 50.03 Pa e 130.09 ± 42.07 a 230.08 ± 95.2 Pa, respetivamente. O comportamento celular nestes hidrogéis demonstrou que enquanto o aumento da concentração de cálcio levou a um aumento do alongamento celular, o aumento da concentração de polímeros teve o efeito

oposto. A variação da concentração do péptido também demonstrou que a adesão celular aumenta à medida que a concentração do peptídeo aumenta, tal como esperado. A deposição fibronectina, um importante componente da MEC, foi também avaliada ao dia 14 de cultura, demonstrando que em hidrogéis preparados a uma concentração de 2% e 3% de polímero as células eram capazes de formar redes celulares interconectadas e secreta grandes quantidades de fibronectina. Por outro lado, os hidrogéis preparados a 4% de polímero restringiram significativamente a deposição de fibronectina. Além disso, foram produzidos esferoides multicelulares de fibroblastos, os quais foram posteriormente incorporados nos hidrogéis para avaliar a migração celular. Foi possível observar uma maior contração do diâmetro dos esferoides nas primeiras 24 horas após as células terem sido cultivadas nos moldes. No entanto, o seu tamanho continuou a diminuir ao longo do período de cultura de 7 dias. Os esferoides permaneceram metabolicamente ativos durante os 7 dias de cultura, embora tenha sido observada uma diminuição na atividade metabólica que está diretamente relacionada com o aumento da densidade celular e do diâmetro do esferoide. Por fim, os esferoides foram incorporados nos hidrogéis para avaliar o comportamento migratório dos fibroblastos. Os resultados indicaram que o aumento da concentração de polímero restringiu severamente a capacidade de os fibroblastos migrarem e invadirem o hidrogel. Para além disso, observou-se que o tempo de maturação dos esferoides não teve um impacto muito significativo na sua migração. Por outro lado, a densidade celular mostrou que, embora os esferoides preparados com 2500 células se tenham desagregado completamente no interior do hidrogel, a densidade celular não foi suficiente para promover a formação de redes celulares interconectadas, enquanto os esferoides com 5000 e 10000 células formaram estas estruturas.

De uma forma geral, foi possível criar um hidrogel com propriedades mecânicas controláveis através da combinação de estratégias de reticulação física e química. Usando este hidrogel, foi possível demonstrar que as propriedades mecânicas desempenham um papel regulatório nas funções de fibroblastos da derme, tais como proliferação, morfologia, migração e deposição de MEC.

This page was intentionally left blank.

Acknowledgments

Com a chegada ao final de uma etapa tão importante, resta-me apenas agradecer às pessoas sem as quais teria sido extremamente difícil terminá-la.

Antes de mais, tenho de agradecer ao meu orientador, Dr. Rúben Pereira, pela oportunidade que me deu, por todo o conhecimento transmitido e pela orientação ao longo de todo o processo da minha dissertação. Para além disso agradeço também à Dr. Flávia Castro pelo apoio prestado e pela orientação ao longo de todo este trabalho.

Devo ainda um enorme obrigada ao Luís por toda a ajuda e cooperação no laboratório, por todos os cafés de manhã e por todas as vezes que me chamaste à razão e me fazes ver o lado positivo das coisas.

Quero ainda agradecer ao Nuno, a pessoa que mais teve de aturar as minhas incertezas e inseguranças, por toda a sua paciência durante estes longos meses e por estar sempre presente quando eu mais precisava.

Obrigado à Carol por ter sido a minha fiel companheira durante estes 5 anos de faculdade e pela interajuda que sempre demonstrámos uma à outra.

Finalmente, às pessoas mais importantes, à minha mãe, ao meu pai e aos meus irmãos, um enorme obrigado por serem os meus maiores apoiantes incondicionais. Sem vocês isto não seria possível.

This page was intentionally left blank.

Table of Contents

List of Figures

List of tables

Abbreviations e Symbols

3D	Three-dimensional
α-SMA	Alpha Smooth Muscle Actin
APG	Apiogalacturonan
BSA	Bovine Serum Albumine
Ca^{2+}	Calcium Ion
$CaCl_2$	Calcium Chloride
CLSM	Confocal Laser Scanning Microscope
CO_2	Carbon dioxide
DAPI	4',6-diamidino-2-phenylindole dihydrochloride
DE	Degree of Esterification
DMEM	Dulbecco's Modified Eagle's Medium
DMTMM	4-(4,6-dimethoxy-1,3,5-triazine-2-yl)-4-methylmorpholinium chloride
ECM	Extracellular Matrix
EDTA	Ethylenediaminetetraacetic Acid
EGF	Epidermal Growth Factor
ELR	Elastin/Laminin Receptor
FAK	Focal Adhesion Kinase
FBS	Fetal Bovine Serum
FGF	Fibroblast Growth Factor
GAG	Glycosaminoglycan
HBSS	Hank's Balanced Salt Solution
HG	Homogalacturonan
HM	High Methoxyl
hNDF	Human Neonatal Dermal Fibroblasts
IGF	Insulin-like Growth Factor
IGF-1	Insulin-like Growth Factor-1
IL-1	Interleukin-1
IL-6	Interleukin-6
LM	Low Methoxyl
MMP	Matrix Metalloproteinases
MEC	Matriz Extracelular
NaCl	Sodium Chloride
NMR	Nuclear Magnetic Resonance
PBS	Phosphate Buffered Saline
PectX	Pectin-based Polymer

PectX-FUR	Furan-Modified Pectin-based Macromer
PectX-MAL	Maleimide-Modified Pectin-based Macromer
PEG	Polyethylene Glycol
PDGF	Platelet-derived Growth Factor
PF4	Platelet Factor 4
PFA	Paraformaldehyde
RGD	Arginyl-glycyl-aspartic acid
RG-I	Rhamnogalacturonan-I
RG-II	Rhamnogalacturonan-II
Rpm	Rotations per minute
TGF-α	Transforming Growth Factor Alpha
TGF-β	Transforming Growth Factor Beta
TSP-d4	3-(trimethylsilyl) propionic-2,2,3,3-d4 acid sodium salt
UV	Ultraviolet
VEGF	Vascular Endothelial Growth Factor
XG	Xylogalacturonan

Chapter 1 – Introduction

1.1. Wound healing and mechanomodulation

Skin is the largest organ of the human body having several essential functions, such as providing the body with a protective barrier, regulating body temperature, sensation, excretion, immunity, blood storage, and vitamin D production [1]. It is a multilayered tissue composed of several cells and ECM components which confer its highly dynamic with specific biochemical and physical properties [2], [3]. Since it is the outermost layer of the human body, it is subject to all sorts of interactions with the external environment which can lead to its damage. Injuries are considered disruptions of the structure and functions of the skin, which can be triggered by a number of different causes, such as surgical incisions or burns. When the skin suffers an injury, it immediately triggers a healing process in order to restore its original structure and functions. This is a highly coordinated and dynamic process in which several biologic systems interact with each other via cellular and molecular mediators [4]. However, in more severe burn wounds, inflammation and skin remodeling are usually prolonged which can lead to the excessive accumulation of ECM components and, consequently, a dysregulation of the collagen synthesis and degradation process, mainly by dermal fibroblasts. In most critical cases, the persistence of macrophages and fibroblasts in the injury site leads to an exaggerated accumulation of collagen, forming hypertrophic or keloid scars [5], [6].

According to the World Health Organization (WHO), over 180,000 people die each year as a consequence of burns, while almost 11 million people worldwide experienced burns severe enough to seek medical attention in 2004 alone. Although the mortality rate has decreased, this leads to an increase in morbidity. In most cases, severe non-fatal burns lead to the need for prolonged hospitalization and hypertrophic or keloid scars formation, resulting in disfigurement and disabilities, which makes them a leading cause of morbidity [7]. Furthermore, the American Burn Association estimated that in 2016 more than 486,000 individuals received medical treatments for burn injuries and that there are at least 40,000 hospitalizations that were a result of this type of wound, in the United States alone [8]. In a study carried out by Guest et al, [9] the costs and outcomes of burn wound management and its progression were analyzed over the course of 24 months. This study allows us to perceive a clear difference between the costs of burns that heal within their normal timeframe and those that do not. During this study, burns that healed within their ideal timeframe had an overall cost of US$15,302.85, while the treatment of those which had a prolonged healing period cost US$51,734.80. Furthermore, it was specified that the total allocated for wound dressings alone was US$589.81 and US$3,288.98 for burns that healed within their normal timeframe and burns that did not, respectively. Moreover, according to a report by Transparency Market Research,

the total costs of burn wound hospitalizations alone were approximately US$1.3 billion in 2018, and in the same year, the global burn treatment market was evaluated to be worth about US$2.6 billion. In addition, they establish that a Compound Annual Growth Rate is expected to be close to 5% between 2019 and 2027, so they predict that this market will be worth about US$4 billion by that year [10]. Thus, severe burns, and more specifically those that do not heal in a short period of time, approximately 30 days [11], resulting in the formation of fibrotic tissue (hypertrophic and keloid scars), are a socio-economic burden.

The "gold-standard" technique for the treatment of severe burn wounds is the use of autografts, as they are obtained from the patient and represent a minimal risk of rejection. However, its main disadvantage is the limited availability, especially in patients with a high total body surface area affected percentage. Other skin grafts, namely allografts and xenografts, despite being more easily available, can induce rejection by the immunological system of the patient and there is also the possibility of disease transmission. Furthermore, scar formation, wound contraction, and a lack of tissue integration are risks usually associated with those grafts [12], [13]. In light of these constraints, skin substitutes are frequently employed to promote burn wound healing. When dealing with severe wounds that damage at least the first two layers of skin, it is important to reconstruct both the dermis and the epidermis in order to accomplish effective wound closure [14]. It is clear to see that even though there have been breakthroughs in skin substitutes, the results in minimizing or eliminating scars have been underperforming. Therefore, further investigation in other fields such as the immunomodulation as well as the mechanomodulation of cells involved in skin repair has recently been the focus of some research works.

Most skin cells are mechanosensitive, capable of perceiving mechanical stimuli applied to their surroundings through several structures termed mechanosensors. These stimuli are translated to biochemical signals, inducing different types of responses from cells, this mechanism is called mechanotransduction [15]. To effectively develop mechanomodulatory dressings, it is necessary to first understand how cells sense and transduce the mechanical properties of the surrounding niche as well as how such mechanical cues drive cellular responses and new tissue formation. Often, excessive scarring occurs when mechanosensitive and mechanoresponsive cells recognize various mechanical stimuli, such as matrix stiffness which can stimulate and activate key mechanosignaling pathways. Currently, research has identified several of these signaling pathways, which are primarily present in fibroblasts, the main cell causing excessive extracellular matrix deposition in pathological scars [16].

Thus, mechanomodulation of the cellular response appears to be a promising approach to address the presented problem of wound healing in severe burns that result in excessive scar tissue formation. However, despite advances in the field, there is still a need for further research to understand how the mechanical properties of cell's microenvironment impact their biological response.

1.2. Aim of the thesis

The main objective of this dissertation was to evaluate how the mechanical cues of a bioengineered hydrogel, aimed to be used as a wound dressing, impact the fibroblast response in 3D.

Specifically, we aimed to:

(i) Develop a viscoelastic hydrogel with adjustable mechanical and biochemical properties, that mimics those of normal skin. A dual crosslinking technique was pursued to better modulate the mechanical characteristics of the hydrogel, which were determined through rheological tests.

(ii) Assess how the mechanical and biochemical properties of the hydrogels influence essential cellular behaviors in individualized cells, such as cell adhesion and spreading. The biocompatibility of these gels was also determined.

(iii) Determine whether cell migration of multicellular fibroblast spheroids is affected by the mechanical properties of the hydrogel as well as by spheroid characteristics.

Chapter 2 - Literature Review

2.1. Skin anatomy, physiology, and healing

2.1.1. Skin structure, functions, and cells

The skin is the largest organ in the human body, providing a protective barrier and regulating essential functions such as body temperature, sensation, immunity, blood storage, and vitamin D. These functions are assured by the three main layers that compose the skin, which are the epidermis, the dermis, and the hypodermis (Figure 1) [17]–[20]. It is important to highlight that there are specialized structures across these layers that impart the regulatory and protective functions of the skin. These are named skin appendages and include structures such as the pilosebaceous follicles, the sweat glands, and the sebaceous glands, which, although they are mainly located in the dermis and hypodermis, are also connected to the epidermis [17], [21].

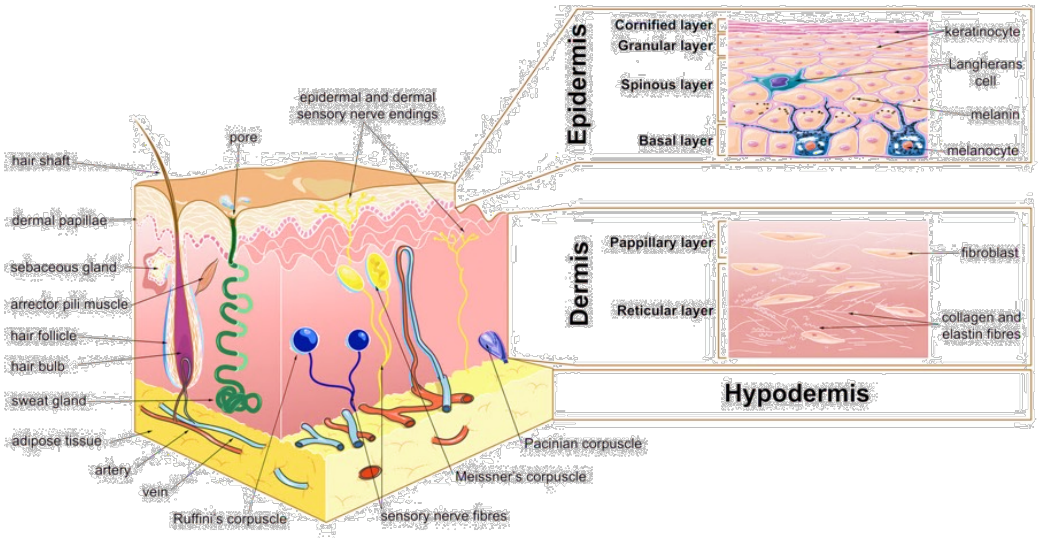

Figure 1 - Schematic representation of the different layers of human skin, including the cells, and appendages [22].

The epidermis is the outer layer, which is in direct contact with the external environment, serving as a protective barrier that shields the body from microorganisms, chemical substances, and physical trauma. Moreover, it limits water loss, maintains optimal hydration, and has sensory functions. This first layer is likewise stratified, with keratinocytes accounting for more than 80% of its cells, but it also contains other cells such as melanocytes, Langerhans cells, and Merkel cells, all of which play important roles in the functions of the epidermis [18], [20]. Keratinocytes are formed from basal cells that divide and subsequently start migrating towards

the skin surface, during which these cells undergo proliferation, differentiation, and keratinization. These cells produce keratin, which imparts strength and protection to the skin, as well as lamellar granules, which release a variety of compounds such as lipids, proteins, and hydrolytic enzymes, all of which contribute to the skin's barrier function [23], [24]. The homeostasis of keratinocytes is crucial in maintaining the skin's protective barrier function and is achieved by their communication and adhesion to each other through intercellular connections formed by desmosomes, which consequently leads to an adequate rate of cell renewal and differentiation [18]. The differentiation, morphology, and location of these cells allow the identification of the epidermis' four or five different layers, depending on body location [25], [26]. As mentioned, this layer is also composed of melanocytes, which are located in the basal layer and are responsible for the production of melanin, a pigment transported to keratinocytes that shields the genetic material in the nucleus from ultraviolet (UV) radiation [8]. Langerhans cells are mainly distributed throughout the spinous and granular layers and are the first immune barrier, as these cells are able to recognize and process antigens by phagocytizing them [23], [27], [28]. Finally, Merkel cells are mechanoreceptors that may be found individually in the epidermis or organized into specialized structures known as tactile discs, playing an important role in the skin's sensory function [23], [24], [27].

Underlying the epidermis is the dermis, and these two skin layers are connected by a specialized structure called the basement membrane that not only attaches them but also provides support for the epidermis. The basal layer of the epidermis is connected to this membrane by hemidesmosomes, which in turn is connected to the papillary dermis by collagen fibrils. The basal membrane is semipermeable, serving as a protective barrier against chemicals and other cells while allowing the diffusion of nutrients and oxygen to the upper layer [29], [30].

The dermis constitutes the thickest skin layer and is mainly comprised of connective tissue consisting of collagen and elastin fibers, which provide the skin flexibility, elasticity, and resistance to mechanical forces. This layer also harbors blood and lymphatic vessels, nerves, and skin appendages such as the sebaceous and sweat gland. Thus, the dermis is also responsible for defending the body from mechanical traumas and assuring thermoregulatory and sensory functions [19], [27]. This layer also comprises fibroblasts, which are the predominant cell type and are responsible for the synthesis of the extracellular matrix (ECM) components. In addition, it also contains macrophages and mast cells, which are involved in the immunological and inflammatory responses [27], [31], [32]. The dermis is comprised of two distinct regions, the papillary and reticular dermis, each with its own composition and function. The papillary layer, which is the most superficial, is thinner and made up of loose connective tissue with some collagen and elastin fibers and a higher cellular density. The reticular dermis, on the other hand, is a thicker and highly organized network of connective tissue, consisting mostly of tightly interwoven elastic fibers and thick dense collagen bundles [28], [29], [33].

The hypodermis is the skin's deepest layer, located directly underneath the dermis. It is mostly composed of adipose tissue and collagen fibers derived from the dermis, enhancing the interconnections between these layers, and is also interlaced with blood and lymphatic vessels and nerves. This layer is a reservoir of energy and fluids, serving as the structural support for the upper layers and aiding in thermoregulation due to its heat-insulating properties [28], [34].

2.1.2. The role of ECM in skin homeostasis and wound healing

2.1.2.1. The ECM, biophysical and biochemical signals

The ECM is an abundant cell-secreted component characterized by its dynamic nature and tissue-specific properties. It is a 3D arrangement of macromolecules that are continuously synthesized, secreted, and remodeled by skin cells, mainly fibroblasts and epithelial cells. The ECM can be described as a gel-like matrix composed of a complex network of collagens, elastin, proteoglycans, glycosaminoglycans, laminins, fibronectin, and matricellular proteins (Figure 2), which are essential to maintain the skin's healthy development and homeostasis and to support wound healing [2], [3]. ECM's primary role is to function as a scaffold, preserving the integrity of cells and tissue structure; however, it also acts as a reservoir of growth factors, cytokines, and chemokines, allowing intracellular transmission of biophysical and biochemical signals toward regulating cell response [35].

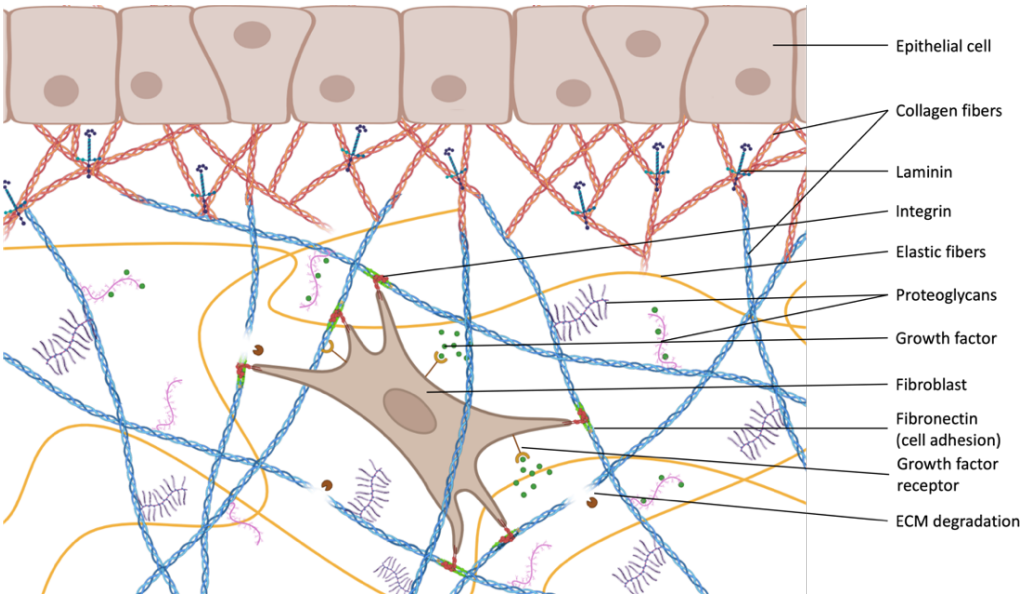

Figure 2 - Schematic representation of the ECM composition and several interactions with the cells. Created at biorender.com.

Collagens are one of the most prevalent components of the ECM, with over 20 subtypes discovered in the skin. These can be classified as (1) fibrillar, which aggregate and

crosslink with one another, producing the structure of the ECM and imparting its tensile strength, and (2) non-fibrillar, which create a reticular network binding with cells and specialized ECM molecules, forming specialized structures such as the basement membrane. Elastin molecules generate elastic fibers through crosslinking with nearby elastin molecules such as fibrillin, a glycoprotein that keeps these fibers unified. Together they interact to provide the ECM its elasticity and flexibility, as well as the capacity to recoil after mechanical stress, proving to be also important components to preserve the ECM's structure [2], [36]. Fibronectin is another glycoprotein found in the ECM that interacts with other extracellular molecules as well as with certain cells via membrane receptors. Cells recognize the arginine-glycine-asparagine (RGD) amino acid sequence, which triggers signaling pathways for cell attachment, migration, and differentiation, therefore playing an important role in cell communication and adhesion [37]. Glycosaminoglycans (GAGs) are negatively charged hydrophilic polysaccharides present in the ECM, such as chondroitin/dermatan sulfate, heparan sulfate, heparin, and hyaluronan. Most GAGs are covalently linked to a protein, forming structures called proteoglycans, such as decorin and versican. Due to the properties of these molecules, they draw ions via osmosis, which consequentially leads to the attraction of water and the entrapment of large volumes in their structure. As a result, they are responsible for maintaining the osmotic balance and hydration of the skin, thus contributing to its compressibility and the viscosity characteristic of the dermal connective tissue. In addition, most are able to bind to growth factors found in the ECM, granting spatiotemporal modulation of these substances [38], [39].

As stated earlier, the ECM is not a static structural scaffold, but instead is a dynamic matrix responsible for the regulation of cell fate through mechanical and biochemical cues essential for tissue development, hemostasis, and regeneration. Cells are capable of binding to the ECM via cell transmembrane receptors such as integrins, allowing them to perceive biophysical cues of their microenvironment, such as stiffness and porosity, and activating a cascade of downstream signals in the cell. ECM also has a role in the spatiotemporal presentation of biochemical signals that are critical for cell behavior. Biochemical cues are often delivered in the form of soluble signals, though the ECM can also bind soluble signals to the cell surface, boosting their effective concentration and limiting their degrees of freedom [40], [41]. Integrins are also able to detect specific ECM components and bind to a wide range of intracellular proteins, enabling interactions with the cells' cytoskeleton and signal transduction pathways. Although integrins are one of the main cellular receptors, other extracellular matrix receptors have been reported such as transmembrane proteoglycans (syndecans, receptor for hyaluronan mediated motility, and CD44), elastin/laminin receptor (ELR), CD36, annexin II, and receptor tyrosine kinases [11], [42]. Apart from signaling through cellular response, the ECM can also signal via the proteolytic cleavage of active components and mechanical exposure of cryptic sites. Overall, when physical or chemical signals from the ECM contact with cells,

they create amplified chemical messages that are subsequently delivered to a decision center, such as the cell nucleus, which determines how the cell should behave [40], [43].

2.1.2.2.Wound healing process

A skin wound is an injury described as a disruption to its normal anatomical structure that comprises the tissue's functions, and it is usually caused by surgical incisions and mechanical, thermal, or chemical injuries. The skin rapidly responds to this disruption by triggering the healing process which aims to restore the original skin anatomy, properties, and functions. This is a highly orchestrated and dynamic process in which both the immunologic and biological systems interact with each other via cellular and molecular mediators [4]. There are four main healing phases that, in an acute wound, occur in the following order: hemostasis, inflammation, proliferation, and remodeling (Figure 3) [44]. Wounds are classified as either acute or chronic based on how long it takes for them to heal. While acute wounds typically take up to 3-4 weeks to heal in an orderly and efficient manner, chronic wounds are difficult to heal injuries that do not heal in an organized or timely manner in a period of 30 days [11].

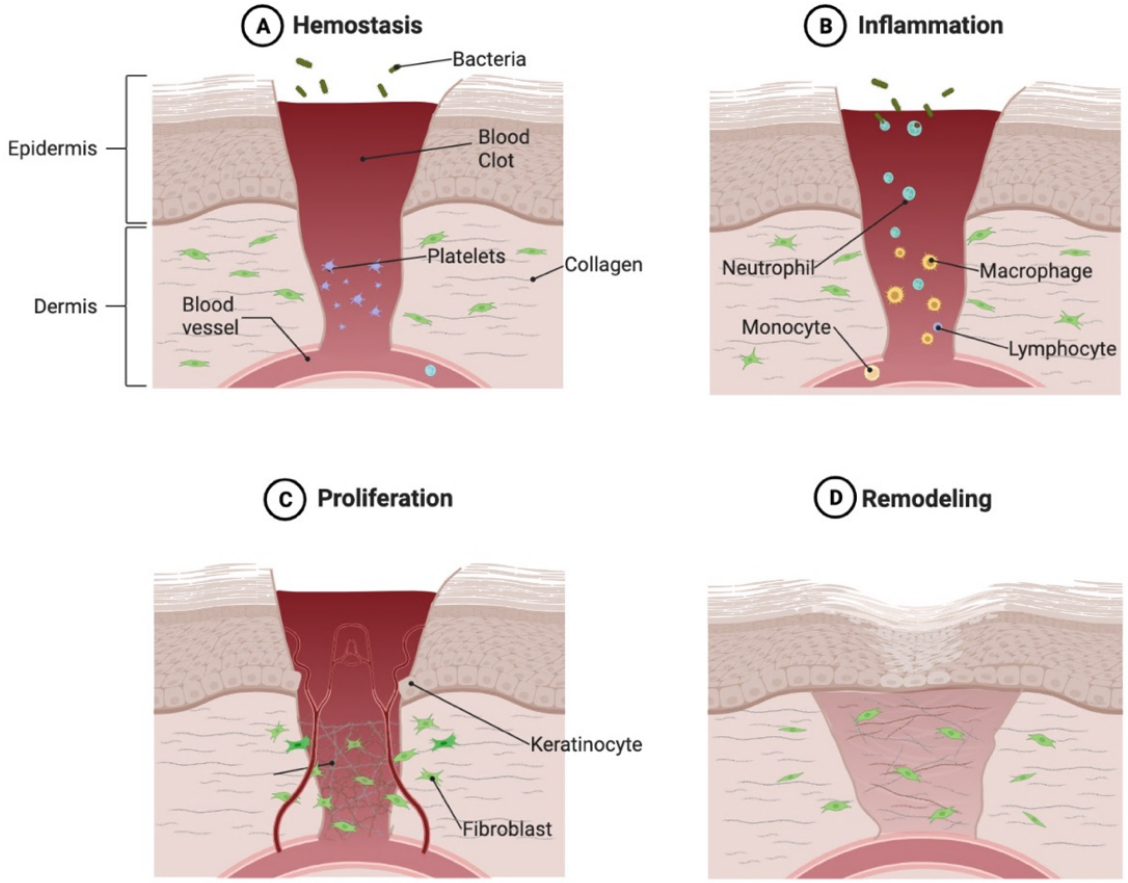

Figure 3 - The healing process of an acute wound. Its four main stages occur in a highly organized manner in the following order: (A) hemostasis, (B) inflammation, (C) proliferation, and (D) remodeling. Created at biorender.com.

In acute wounds, the first phase of the healing process starts immediately upon injury, when the blood components and platelets come in contact with the exposed collagen from the ECM, leading to the formation of a clot that provides a provisional matrix for wound protection and cell migration. This clot is composed of fibronectin, fibrin, vitronectin, and thrombospondin [45], [46]. The aggregated platelets degranulate and release key mediators such as platelet factor 4 (PF4), platelet-derived growth factor (PDGF), insulin-like growth factors (IGFs), epidermal growth factor (EGF), and transforming growth factor alpha and beta (TGF-α and TGF-β). These mediators allure and activate fibroblasts, endothelial cells, and macrophages, which are critical for the next stages of the healing process [45].

The inflammatory stage starts with the lure of leukocytes or neutrophils, which are the first cells to infiltrate the wound site and begin to phagocytose bacteria, foreign particles, and damaged tissue. Monocytes are then recruited to the wound site, through mediators and degraded ECM components, which, upon arrival, connect to the ECM and differentiate into macrophages [5], [47], [48]. These take over the neutrophil's functions, keeping the wound clear of any bacteria and necrotic tissue, through phagocytosis and the synthesis of enzymes such as collagenase and elastase. Macrophages have a crucial role in the progression of the wound healing process, as they release cytokines and growth factors, such as PDGF, fibroblast growth factor (FGF), vascular endothelial growth factor (VEGF), interleukin-1 (IL-1) and interleukin-6 (IL-6), IGF-1, and TGF-β and TGF-α, attracting and activating fibroblasts, endothelial cells and promoting angiogenesis, which ultimately leads to the transition to the next phase [45], [48]. Lastly, lymphocytes are the final cells to emerge during the inflammation, and they participate in cellular immunity and antibody production. Moreover, lymphocytes provide important profibrotic cytokines and growth factors [46], [49].

The proliferative phase is reached when the wound starts being reconstructed with new tissue. In this stage, it is possible to observe several events such as fibroblast migration, collagen synthesis, *de novo* ECM formation, angiogenesis, granulation tissue formation, epithelialization, and wound contraction. In order to carry out the repair of the skin's wound, it is fundamental that a continuous supply of nutrients is provided. Therefore, angiogenesis is triggered, repairing affected blood vessels, and creating new ones towards the wound center [50], [51]. Meanwhile, fibroblasts begin replacing the provisional matrix with a collagen-rich granulation tissue, which is achieved by breaking down the provisional matrix and synthesizing important components for the new ECM, such as fibronectin, proteoglycans, glycosaminoglycans (hyaluronan) and glycoproteins (collagen, mainly type III, and elastin) [4], [51]. Fibroblasts also differentiate into myofibroblasts which are important not only because they secrete various components of the ECM, but also promote wound contraction, this way approximating the wound edges and diminishing the healing time. Myofibroblasts express smooth muscle actin (α-SMA) which confers a contractile behavior and allows them to bind to ECM via the integrin receptors. These cells gather at the wound edge, attaching to the matrix

and contracting it to decrease the size of the wound [50]–[53]. At the same time, keratinocytes in the vicinity of the wound are stimulated by growth factors to proliferate and migrate towards restoring the epidermis, promoting reepithelization. These epidermal cells shape the new basal membrane and when cells from different edges of the wound come in contact, a signal is transmitted to end the migration and link themselves to each other for stabilization [51], [54].

In the last phase of wound healing, remodeling, the ECM continues to balance the synthesis and degradation of collagen, in order to remodel the matrix. Macrophages and fibroblasts lead to the degradation of collagen, with the production of matrix metalloproteinases (MMPs). Meanwhile, collagen is being synthesized, replacing collagen type III with type I, and crosslinked by an enzyme, in order to achieve the organization and strength as close to native skin as possible [45], [50]. In this phase, it is also possible to observe a decrease in the number of cells present, as a result of apoptosis, and a regression of the blood vessels from angiogenesis [55]. Despite the continuous remodeling process in wound healing, scar development is the most common consequence of this process, and scars typically only achieve around 70% of the tensile strength of the unwounded tissue [56].

In more severe injuries, such as partial and full-thickness burns, there is a high risk of hypertrophic or keloid scars formation, which can lead to considerable morbidity as they induce a variety of severe symptoms such as soreness, itchiness, dyspigmentation, heat sensitivity, and decreased range of motion related to its contraction [57]–[59]. Partial and full-thickness burns affect both the dermis and the epidermis and can even reach the hypodermis, which can lead to abnormalities in the wound healing process [60], [61]. These two types of scars are caused by excessive scarring due to an imbalance of fibrosis, which is the collagen turnover process in which fibroblasts replace type III collagen with type I collagen [6]. The inflammation and skin regeneration processes are prolonged in these wounds (Figure 4), resulting in a buildup of ECM components and, consequentially, a dysregulation of the collagen synthesis and degradation processes. As a result, there is a persistent presence of macrophages and fibroblasts which ultimately lead to an exaggerated accumulation of collagen [5], [6]. In this context, the amount of collagen in hypertrophic scars and keloids is significantly higher than in normal skin, and the ratio of type I to type III also fluctuates among them. Furthermore, the wound mechanical environment, such as the physical properties of the ECM, has been shown to influence wound healing and scar formation as it modulates cell behavior [62], [63].

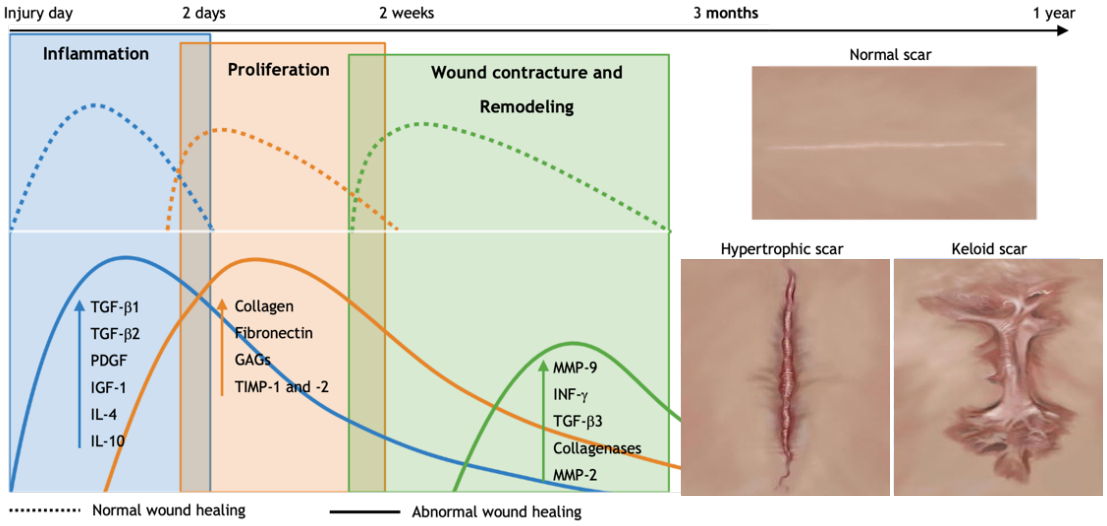

Figure 4 - Differences between normal and abnormal wound healing leading to excessive scar formation over time. Normal wound healing follows a time-specific sequence of phases whereas excessive scar formation exhibits dysregulations of the fundamental signaling pathways, which can result in persistent inflammation, excessive collagen synthesis, or inadequate matrix degradation and remodeling [62], [63].

2.2. The importance of mechanical forces in dermal fibroblast biology

2.2.1. General principles in mechanotransduction

Mechanotransduction is defined as the process through which cells detect mechanical stimuli from their microenvironment, such as load, deformation, stiffness, roughness, or topography, and convert them into biochemical signals, resulting in a modulation of the cell's response. There are a variety of mechanosensitive and mechanoresponsive cells capable of sensing these cues and activating, suppressing, or even modulating important molecules in mechano-signaling pathways [16], [64]. Fibroblasts are one of the most abundant mechanoresponsive cells in the skin and are able to detect these stimuli through structures named mechanosensors, including the cells membrane, mechanosensitive ion channels, integrins, focal adhesions, and protein and intercellular complexes. There have been several mechanotransduction pathways reported throughout the years, such as the integrin, Mitogen-activated protein kinase (MAPK), Yes-Associated Protein (YAP)/Tafazzin (TAZ), Wingless-related integration site (Wnt), Roh, Smad, and FAK signaling pathways (Figure 5) [15].

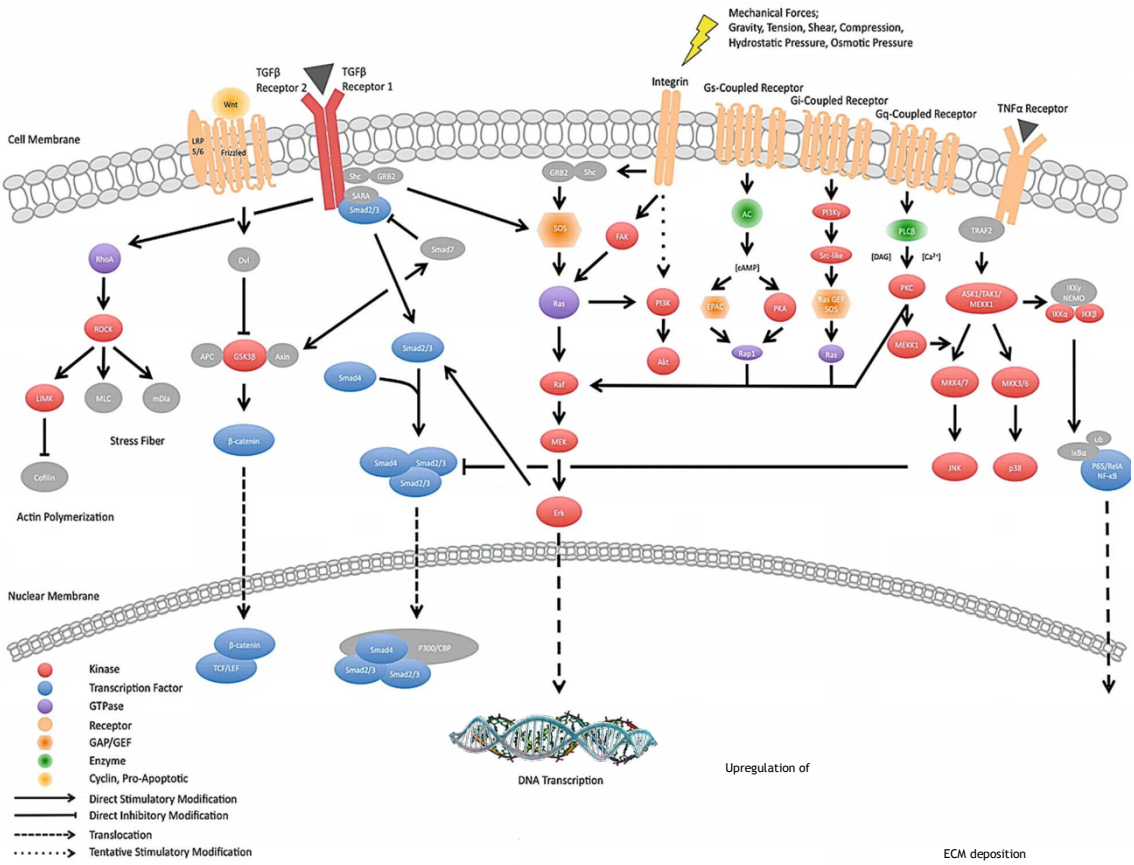

Figure 5 - Mechanosignaling pathways activated in cells when subjected to mechanical stress. When mechanosensors in or on cells are engaged, multiple mechanosignaling pathways are activated, which subsequently affect cell response [15].

The integrin-FAK route is one of the most typical mechanotransduction mechanisms that can affect fibroblast survival, collagen synthesis and reorientation, and its differentiation into myofibroblasts. The mechanical stimuli are received and conveyed from the cell surface to cell-matrix adhesion sites on the cell membrane through the ECM. When the integrin receptors bind to ECM, they are activated and their molecular form is altered. When integrin receptors link to ECM components such as fibronectin, their molecular structure changes, allowing their cytoplasmic tails to engage with adaptor proteins that bind them to cytoskeletal actin. These proteins form the focal adhesion complex that physically binds the integrins to the ends of the contractile microfilament bundles, establishing a molecular connection between the ECM and the cytoskeleton. These complexes stimulate focal adhesion kinase (FAK), which is essential for cell migration. Their activity triggers intracellular signal transduction pathways, which enhance the renewal of cell-ECM interactions. In wound healing, when FAK is suppressed or removed, pro-inflammatory and pro-fibrotic growth factors are significantly attenuated, and as a result collagen, deposition, and myofibroblast quantities are decreased [16], [65]. Another significant mechanotransduction mechanism implicated in fibrogenesis is the integrin-mediated TGF-β pathway. It is a soluble factor that can trigger

fibrosis and modulate myofibroblast differentiation as it is involved in cell structural changes and the release of pro-fibrotic molecules such as α-SMA, which interact with myosin to generate tension. TGF-β pathways are distributed downstream through the Smads pathway and combine with Co-Smad to reach the nucleus, where they bind DNA and activate target genes. TGF-β1 also increases myofibroblast contractility and stimulates the synthesis of fibronectin fibrils, which is associated with pathological contracture. Furthermore, ECM stiffness influences induced TGF-β1 expression and consequently differentiation of fibroblasts into myofibroblasts, as integrins are activated and release this factor in stiffer matrices. This leads to an increase in smooth muscle actin, which results in greater ECM stiffness and a positive feedback loop for fibrosis. Moreover, TGF-β2 and TGF-β3 are known to have pro-fibrotic characteristics and regulate epidermal and dermal cell motility, respectively, and hence play a significant role in wound healing [65]–[67].

2.2.2. Skin viscoelasticity

Viscoelasticity is considered to be a universal and fundamental characteristic of most biological tissues, as it allows the tissues to undergo deformations without compromising their integrity and the skin is no exception. The primary components of the ECM, as well as the resident cells, are responsible for this viscoelastic behavior of skin [68]. Viscoelastic materials are characterized as exhibiting the behavior of both elastic materials and viscous liquids when subjected to mechanical forces. When exposed to stress, which is defined as the force or pressure per unit area of a material caused by external loads or forces, purely elastic materials demonstrate the capacity to alter their length, volume, or shape followed by recovery to their original state once the stimulus is withdrawn. Viscous liquids, on the other hand, react the completely opposite way, deforming in a steady, time-dependent, and permanent manner, unable to restore to their previous shape. As a result of their in-between mechanical properties, viscoelastic materials display an initial elastic response when a force is applied to them, allowing them to store the applied stress; however, this is followed by a time-dependent response and energy dissipation. If subjected to external stress or load, these materials will creep, described as the material's tendency to slowly deform, and as a result of stress exposure, they will experience stress relaxation, meaning that the force required to maintain the deformation will progressively decrease. Furthermore, when a sinusoidal tension is applied, stress and strain, which is the amount of deformation a material undergoes, are considered to be in-phase for purely elastic materials since the entire imposed energy is stored and later recovered with no loss; however, viscous fluids are found to be completely out of phase, which means that all of the energy is dissipated and lost through internal friction in the system [68]–[71].

As previously described, the skin is a dynamic tissue whose chemical and physical properties are strongly influenced by age, gender, ethnicity, and location, among other factors. It mainly

consists of a collagen-rich fibrous network embedded in ground substance. On one hand, the main fibrous constituents of the ECM, namely collagen and elastin, are the key players which provide the structural stiffness and elasticity of the skin, with elasticity fluctuating depending on the direction of force application due to the alignment of the fibers. The bonds that crosslink these fibers in the ECM are usually non-covalent weak bonds that allow the dissipation of energy in a time-dependent manner and upon load/deformation application, as these can break the bonds. On the other hand, this proteoglycan-rich ground substance is another main participant in providing skin its viscous nature, as its water uptake largely influences the energy loss through its flow in and out of the matrix [68], [72]. In this way, the skin exhibits anisotropic, time-dependent, viscoelastic material behavior Thus, the skin exhibits an anisotropic, time-dependent behavior of a viscoelastic material with elastic and viscous modulus, as shown in Table 1, which depends on the skin site and also vary with whether or not epidermis is included in the tests. Furthermore, the biomechanics of healthy skin and scar tissue differ significantly. As mentioned, undamaged healthy skin is viscoelastic by nature, whereas scar tissue is typically stiffer and less viscoelastic. As the content and arrangement of dermal fibrous ECM molecules govern skin mechanical characteristics, a dysregulation of ECM composition, abundance, and organization affects not only the mechanical characteristics of the matrix but also the overall mechanics of the tissue, which ultimately will influence cellular signaling [71].

Overall, biomechanical tensile testing, in which the tissue is stretched and the force it generates is quantified, has contributed significantly to the understanding of some aspects of the mechanical behavior of skin. However, the viscoelastic performance of the skin at low loads, which has not been as deeply explored, has been gaining some interest due to its important role in the normal physiological function of this tissue. These studies allow a better characterization of the physical properties of skin, providing insight into its ability to resist stretching, withstand stress, and dissipate energy through viscous methods. These properties can be applied to the development of biomimetic materials with mechanical properties that more closely resemble those of the skin and/or its ECM and be used to study how these characteristics influence wound healing/scar formation and affect the cellular response, and ultimately be employed in the development of wound healing treatments and skin substitutes [15], [71].

Table 1 - Mechanical properties of the human healthy and scarred skin.

Sample composition	*Tissue Condition*	*Testing Method*	*Main Findings*	*Refs.*
Full Skin (Dermis + Epidermis)	Unwounded	Frequency sweep measurements (strain 0.5% and frequencies between 0.628 and 75.398rad/s)	G' ranged from 325.0 to 1227.9 Pa G'' ranged from 68.5 to 189.9 Pa	[73]
Dermis Only	Unwounded	Frequency sweep measurements (strain 0.5% and frequencies between 0.628 and 75.398rad/s)	G' ranged from 434.9 to 6620.0 Pa G'' ranged from 126.3 to 458.6 Pa	[73]

2.3.Hydrogels as ECM-mimics for skin applications

2.3.1. Hydrogels: fundamental concepts

Hydrogels are 3D water-swollen networks formed by the crosslinking of hydrophilic polymer chains, that are capable of retaining large quantities of water or other biological fluids without being dissolved. Hydrogels are porous, permeable structures that facilitate the flow of nutrients, oxygen, and cellular waste, and they also demonstrate swelling ability and viscoelastic properties. Hydrogels may be fabricated using various crosslinking reactions and exhibit adjustable physicochemical features as well as high biomimicry of the ECM of natural tissues. Furthermore, hydrogels can be modified with chemically and physiologically active recognition cues such as stimuli-responsive compounds and growth factors to improve their biofunctionality. The microenvironment provided by hydrogels, more specifically the biophysical/biochemical properties, can significantly affect cell proliferation and differentiation, and also ECM production. Due to the distinctive properties with which hydrogels can be produced, they have been widely studied for various biomedical and tissue regeneration applications, including wound healing [74], [75].

The polymers employed can be either of natural origin, such as polysaccharides derived from animal, plant, or microorganism sources, polynucleotides, and polypeptides, or of synthetic origin, artificially man-made. Naturally occurring polymers usually include carbohydrates and proteins, providing structural support to the plants/animals, hence their biocompatibility and non-cytotoxic effect compared with synthetic hydrogels, which most times are prepared through the use of chemical agents. Moreover, most natural polymers are readily available and cheaper and exhibit bioactive properties [76]. To form hydrogels, polymer chains can be chemically crosslinked, usually through covalent bonds, or physically crosslinked by non-covalent bonds such as molecular entanglement, hydrogen, or ionic bonds, or even a combination of both. The stability of these crosslinks can be tuned by several different methods, such as the use of temperature, ions, or UV radiation.

When designing a hydrogel for wound healing applications, various factors must be taken into consideration, including biocompatibility, biodegradability, bioadhesiveness, and cell-hydrogel interaction. Furthermore, properties such as vascularization capability, antibacterial, anti-inflammatory, and pro-angiogenic qualities may be incorporated into hydrogels, depending on the application. Biocompatibility is a critical necessity for any hydrogel in order to preserve tissue homeostasis by offering an appropriate scaffold without triggering adverse responses. The biodegradability of the hydrogels is also crucial because they serve only as a temporary matrix for skin cell adhesion, proliferation, re-epithelialization and neovascularization, and wound healing. Bioadhesivity also contributes to the long-term durability of hydrogel dressings around the wound area by promoting homeostasis, keeping the site moist, and absorbing tissue exudates during healing [77].

Hydrogels are extensively employed in tissue engineering not only due to the features mentioned above but also for their mechanical and structural properties that are comparable to numerous tissues and ECM, as well as their ability to be given in a non-invasive manner. As a result, producing scaffolds that match both the structure and bio-functions of the natural ECM is extremely desirable [78].

2.3.1.1.Pectin-based hydrogels

Pectin is a naturally occurring polysaccharide, which makes up the structural component of the plant's cell walls and can be extracted from apple pomace and citrus peels, being one of the major by-products of cider or juice industries. It has been widely used in the food industry for its gelling, thickening, and emulsifying capacities. However, it is being increasingly found in pharmaceutical and biomedical applications, owing to its chemical versatility, anionic nature, and ionic crosslinking ability [79], [80].

This polysaccharide is composed mostly of galacturonic acid (70%), rhamnose, galactose, and arabinose (Figure 6), and is regarded as one of the most structurally complex natural polymers. Its backbone is comprised of linear chains (1,4)-a-d-galacturonic acid (GalA) residues which can be acetylated, or methyl esterified. The amount of carboxyl groups esterified with methyl groups determines the degree of esterification (DE) and depending on its DE pectin can be categorized as low methoxyl (LM), with a DE lower than 50%, and high methoxyl (HM), with a DE higher than 50%. These present dissimilar properties, affecting characteristics such as solubility, crosslinking ability, and gel formation. HM pectin is normally soluble in hot water containing a dispersion agent to prevent agglomeration. Furthermore, its gelling usually involves an acidic aqueous media as well as an abundance of carbohydrates. Gelation of HM pectin occurs via hydrogen bonds between non-dissociated carboxyl groups and secondary alcohol groups, as well as via hydrophobic interactions between methoxyl groups and water. On the other hand, LM pectin is not as pH sensitive and its gelling may occur at physiological temperatures and pH values, requiring only the introduction of divalent cations such as calcium, resulting in a spreadable, shear reversible ionically crosslinked gel network [81], [82]. Due to the high complexity of pectin, its exact chemical composition and structure are still under debate, although it is believed that it is composed of three main domains, namely the homogalacturonan (HG) which is usually alternated by rhamnogalacturonan-I (RG-I) and rhamnogalacturonan-II (RG-II). However, other structural classes such as xylogalacturonan (XG) and apiogalacturonan (APG), can also be found in their composition. The HG accounts for at least 65% of the pectin and is known as the smooth area since it is a homopolymer of GalA with no side chains. On the other hand, the remaining domains are considered the hairy region of this polysaccharide due to the occurrence of side chains of different sugars [82], [83].

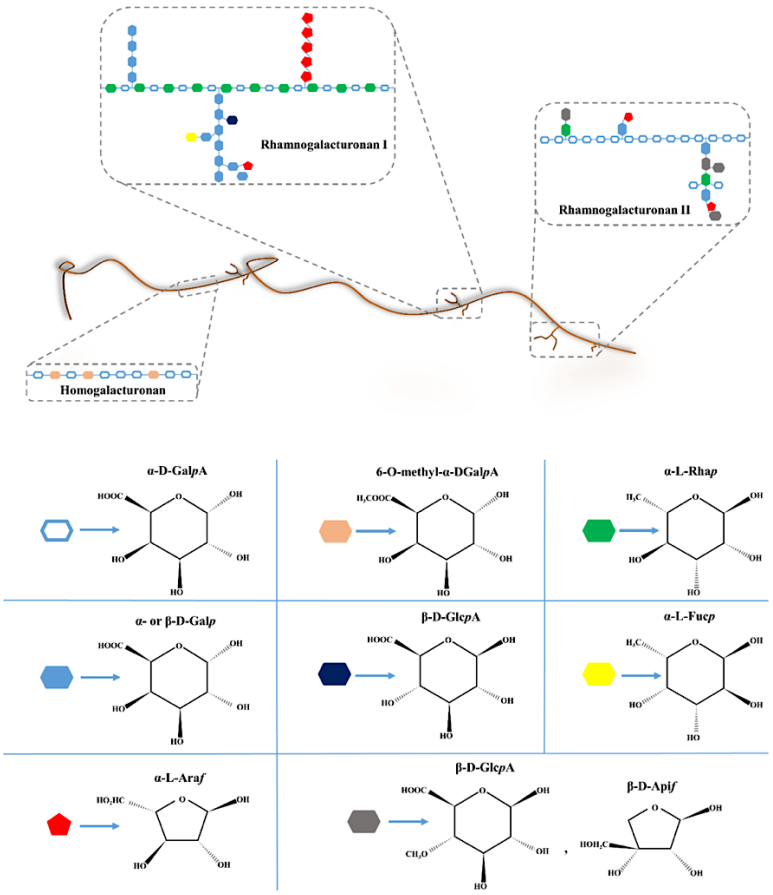

Figure 6 - Schematic representation of the pectin structure. Its smooth zone is composed of partially esterified HG and its hairy zones are composed of highly branched zones namely RG-I and RG-II [84].

Pectin has been shown to exhibit a wide range of bioactive attributes, including anti-tumor, anti-inflammatory, antioxidant, mucoadhesiveness, and biodegradability, among others, which have proven attractive for various biomedical applications, including tissue engineering and regenerative medicine [85]. Aside from these distinguishing characteristics, the presence of numerous hydroxyl, carboxyl, carbomethoxy, and acylamino functional groups make pectin capable to obtain a broad spectrum of derivatives, making it a is a highly versatile material whose viscoelastic properties can be easily modulated and tuned through polymer concentration, crosslinking, or even through its chemical modification [86], [87]. One of the major drawbacks of utilizing pectin polymers for tissue engineering applications is that it exhibits poor cell adhesion, essential for cell survival, mostly owing to their hydrophilic nature. However, the incorporation of cell adhesion sites through the modification of this polymer with oligopeptides containing the RGD sequence has been used to enhance integrin-dependent cell adhesion, one of the most important contributors to the regulation of cell function. As a result, pectin can be used for the production of biomimetic materials for a wide range of natural tissues and may be employed as a matrix to entrap and distribute a range of medicines, proteins, and cells.

2.3.2. The emerging role of hydrogel viscoelasticity in cell response

Most human tissues are viscoelastic being capable of dissipating as well as storing stress. Indeed, this viscoelastic nature of the tissues has been shown to be significant in influencing cell and tissue response, such as in the tendons, skin, and brain. There have been studies that show the pivotal role of tissue viscoelasticity not just in normal physiological processes, but also in disease development. The effect of viscoelastic properties of the cell's microenvironment has been studied both on two-dimensional (2D) and 3D matrices.

In a study, fibroblasts were cultured on 2D alginate hydrogels that were only chemically (covalent bonds) or physically (non-covalent bonds) crosslinked, and RGD was also incorporated into them to promote cell adhesion. The first hydrogels presented purely elastic characteristics and the cells were unable to spread throughout the matrix, presenting a spherical morphology. The latter, however, displayed viscoelastic properties which allowed the cells to spread, presenting a more elongated morphology. Moreover, in the latter, the cells exhibited robust focal adhesions and stress fibers and activation of the transcriptional regulatory protein YAP, a behavior that compares to that seen in the presence of rigid, elastic substrates. This behavior was attributed to the plastic deformation that these hydrogels demonstrated [88]. In another study, performed on purely viscoelastic arrays of polyacrylamide gels with linear acrylamide chains, it was shown that increasing the elastic modulus decreased the stiffness of the fibroblasts and also increased their spreading [68]. Although these studies in 2D cultures are relevant to understand how the viscoelastic properties of the material can affect the cells, it is still known that the dimensionality of the culture affects several parameters such as cell structure and adhesion, signaling, and nutrient transport into the culture. It is known that the dimensionality of the cell culture influences many cellular mechanisms such as cell structure, adhesion, signaling, and even nutrient transport. In order to effectively study cellular behavior, 3D matrices are important since they replicate the native conditions of the cells with greater similarity. A study conducted on 3D hyaluronic acid and collagen interpenetrating network hydrogels, which goal was to recapitulate ECM viscoelasticity and fibrillar architecture, demonstrated that the dynamic crosslinking conferred the hydrogels with stress-relaxation behavior and resulted in a significant increase on fibroblast's spreading and proliferation, as well as the formation of focal adhesions. In this study, the formation of focal adhesions was attributed to the viscoelastic properties of hydrogels but also suggested that the fibrillar component plays an important role in focal adhesion formation [88].

The biochemical and biophysical features of the ECM govern diverse cellular processes not only in 3D space but also in a time-dependent way. Thus, hydrogels should match the tissue-specific and dynamic structural features of natural ECM in order to efficiently support the activities of encapsulated cells in 3D space. Furthermore, changes in cell shape are linked to cell mechanotransduction signaling, which regulates a number of cell activities such as adhesion, migration, proliferation, differentiation, and death. As a result, the dynamic and

adaptive structures of ECM are crucial to a range of activities such as wound healing and tissue regeneration. Dynamic hydrogels have been recently mentioned and are gaining increasing interest, as they are matrixes with temporal and spatial accuracy in response to specific mechanical stresses and biological signals. An example of these are dynamic matrices generated through dynamic crosslinks, that can be cleaved and re-established favoring cell spreading and migration. Recently, numerous types of dynamically chemical and physical crosslinking strategies are increasingly being employed for the production of these dynamic hydrogels as they are usually reversible, and contribute in a degradation-independent to the structural dynamics of hydrogels [70], [89], [90].

2.3.3. Crosslinking reactions to engineer viscoelastic hydrogels

Polymers are usually soluble in an aqueous media; hence it is essential to provide physical and/or chemical crosslinks between polymer chains, in order to preserve the integrity and stability of the produced hydrogels. Crosslinking can be widely defined as the establishment of junction points where the polymer's chains crossover leading to the development of networks that ultimately can result in the formation of hydrogels by restricting the mobility and freedom of polymer chains as well as lowering their solubility. Thus, crosslinking between polymer chains affects important physical properties of the hydrogels produced, such as their elasticity, viscosity, solubility, and swelling ability, among others [91], [92].

As previously stated, the crosslinking can be either of chemical or physical nature, or even a dual crosslinking strategy can be employed, exploiting a combination of both. Chemical crosslinking often entails the generation of covalent bonds between polymer chains, which usually require polymer modification/functionalization. Chemical crosslinking can be divided into several categories depending on the method of crosslinking, such as free radical chain polymerization (e.g., photopolymerization, oxidative–reductive mechanisms), enzyme-catalyzed reactions, "click" chemistry (e.g., thiol-ene radical addition, Michael addition) and dynamic covalent crosslinking (e.g., Schiff Base and Diels-Alder reactions) [92]. While physical hydrogels show stress-relaxing properties, static covalent crosslinks frequently result in purely elastic gels. On the other hand, dynamic covalent chemistry, as an intermediate, may develop viscoelastic materials that exhibit stress-relaxing characteristics and deform under stress to support biological activities such as spreading, proliferation, and differentiation [89]. Chemically crosslinked hydrogels are often defined as permanent, meaning that when cleaved, covalent bonds are unable to reestablish themselves; however, dynamic covalent crosslinking has a reconfigurable character, which means that these chemical connections can rapidly dissociate, following by association upon stimuli removal. Physical crosslinking, on the other hand, often make use of non-covalent interactions which are usually reversible. Physically crosslinked hydrogels can be produced by applying methods such as ionic/electrostatic interactions, hydrogen bonds, hydrophobic interactions (thermally or ultrasonically induced),

chain entanglement, and crystallization, among others [93]. In general, chemically cross-linked hydrogels appear to have more tunable physicochemical properties and exhibit high stability and superior mechanical properties when compared to physically crosslinked hydrogels [74]. However, a significant disadvantage of chemical crosslinking is that many of the available reactions require the use of crosslinking agents that are cytotoxic, therefore, preclude the crosslinking in presence of cells and must be eliminated before application. Physical crosslinking has the advantage of being simple synthesis procedures that do not involve chemical modification or the use of these. However, hydrogels produced using these methods often demonstrate relatively low mechanical stability [93], [94].

Despite the benefits of both physical and chemical crosslinking, some attributes require improvement, such as the potential toxicity of excess and/or unreacted chemicals in the covalent crosslinking reaction, as well as the mechanical strength and environmental responsiveness of physical forces. As a result, dual crosslinking techniques, which combine physical and chemical crosslinking methods, result in hydrogels containing both covalent and physical crosslinks. The former sufficiently contributes to the mechanical strength of the hydrogel, while the latter allows the hydrogel to dissipate greater quantities of energy during deformation, further enhancing the hydrogel's toughness [95].

2.3.3.1.Ionic crosslinking

Ionic interactions are one of the simpler methods for hydrogel crosslinking. In ionically crosslinked hydrogels, the driving force is the electrostatic interactions that occur between oppositely charged molecules. Thus, this method may proceed between ionic complementary polypeptides, two polyelectrolytes with opposite charges, or charged polysaccharide multivalent counterions [96].

The ionic crosslinking method that employs the addition of multivalent counterions to a polymer solution to induce their gelation, is widely used since it is usually a biocompatible process that can occur at room temperature and physiological pH and can easily be reversed by the use of chelating agents, such as ethylenediaminetetraacetic acid (EDTA) and sodium citrate. However, as with most physical crosslinking processes, the hydrogels produced by this method typically exhibit poor mechanical properties. Moreover, the approach poses the possibility of ions being released, which in high quantities might become toxic to the cells [92], [97]. This method frequently involves the usage of multivalent cations, requiring the employment of anionic polymers. Due to this restriction, the approach is fairly limited in terms of polymers to which it may be implemented, some of which are alginate, hyaluronic acid, (low methoxyl) pectin, and gellan gum. In addition, calcium is one of the most commonly employed ions for ionic crosslinking, and among the several water-soluble calcium salts, calcium chloride ($CaCl_2$) is the most frequently applied ionic crosslinker due to its increased solubility in aqueous conditions, resulting in a fast gelation [92], [98]. Upon dissolution in water, the anionic

polymers are ionized, and the carboxylic groups present on their chains generate COO^- groups capable of binding to the multivalent cations via electrostatic interactions [96]. In polymers such as pectin and alginate, these interactions form an egg-box model as can be seen in Figure 7 [99].

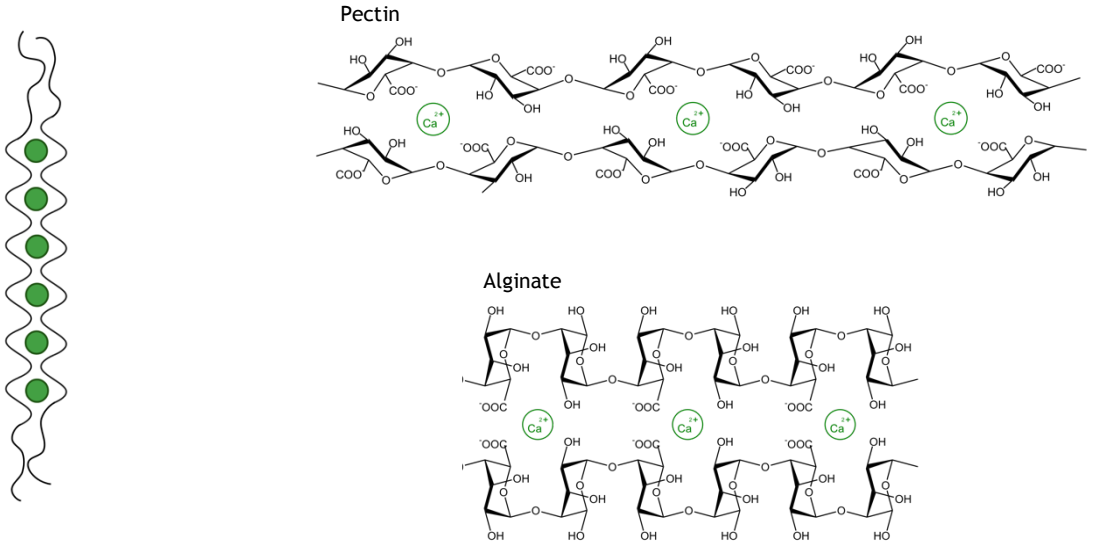

Figure 7 – Schematic representation of the ionic crosslinking of pectin and alginate through electrostatic interactions with Ca^{2+} creating the egg-box model.

The method of preparing hydrogels through ionic crosslinking via multivalent ions and charged polymers significantly influences their gelation as well as the characteristics of the resulting hydrogel. This crosslinking procedure may be carried out in two different manners, through internal and external gelation. On one hand, the ionic solution may be introduced and dissolved directly into the hydrogel precursor solution, on the other hand, the polymer solution may be added to an ion-containing bath, allowing free diffusion of ions into it. Both methods result in the gelation of the polymer solution and the formation of an ionically crosslinked hydrogel. On the one hand, hydrogels synthesized by this first technique generally demonstrate a homogenous structure; yet, they have a looser network and consequently inferior mechanical characteristics. In addition, with this method, the gelation time of the polymer solution for the formation of hydrogels is considerably longer. On the other hand, gels prepared by the second method generally do not have such a homogeneous structure, since the concentration of ions at the surface is considerably higher than in the center, and for this reason, they have been highly regarded for drug loading and release [100], [101].

2.3.3.2.Diels-Alder reaction

Dynamic covalent bonds are a class of reversible chemical bonds that can be broken and reformed under equilibrium conditions, one which the Diels-Alder (DA) reaction falls upon. DA reactions are described as reversible click chemistries of [4+2]-cycloaddition that usually happens between an electron-rich diene and an electron-poor dienophile, to form substituted cyclohexene derivative, leading to the formation of more energetically stable bonds [89], [92]. This reaction is characterized as a click reaction, due to its high selectivity and yields. Furthermore, these reactions can take place in the absence of toxic solvents, other crosslinkers, or catalysts without the formation of by-products or the occurrence of side reactions. However, compared to other click chemistries available, DA reaction is usually much slower, taking longer times for the gelation to occur [102]–[104].

The most common strategy to fabricate hydrogels via DA reaction is to firstly functionalize the hydrogels precursors with the required functional groups and then mix these solutions, where the polymers are crosslinked through the DA reaction, in which diene-dienophile systems that bond in a thermo-responsive way, forming the hydrogels. Among several available diene-dienophile systems, the furan and maleimide groups are one of the most widely utilized conjugates to stimulate this reaction, due to their relatively fast reaction rate at physiological temperatures, as illustrated in Figure 8. Polymers must initially be functionalized with the diene and/or dienophile groups. Chemical modifications, such as amidation reaction, etherification, and imine formation, among others, are frequently required for the coupling of these groups into the polymer chains. The produced hydrogels are typically thermo- and pH-responsive and have been investigated for a variety of biological applications including tissue engineering, drug delivery, and antimicrobial coatings [93], [105]. Gelling rates are typically enhanced in aqueous conditions due to hydrophobic interactions between the diene-dienophile conjugation; however, maleimide groups are susceptible to hydrolysis, which may eventually inhibit the further reaction, affecting the stability of Diels-Alder cross-linked hydrogels. Since the maleimide groups are usually more stable under more acidic conditions, the DA reaction is often carried out in acidic aqueous media which also stimulates a more accelerated DA; nevertheless, these are usually cytotoxic to cells and not adequate for in situ applications. As a result, in recent years, methylfurans have been employed in place of furans to enhance the gelation process at physiological pH, as they offer a more electron-rich diene. However, even though the gelation is enhanced, so is the reverse DA reaction (retro DA). The retro-DA reaction, which is usually favored by increased temperatures, also occurs more readily, which further reduces the stability of the hydrogel. As mentioned, the DA reactions are thermosensitive systems and demonstrate increased reversibility at higher temperatures, usually over 100°C. However, the range of favorable temperatures upon which the DA and retro-DA reactions occur may be adjusted by varying the diene-dienophile conjugation, their concentration, and molecular weight [89], [93], [103], [104].

Overall, DA reactions in the hydrogel synthesis have attracted significant attention for their use in biomedical applications, especially due to their thermal self-healing, reversible properties, and the ease of tuning their bulk characteristics, having also demonstrated the possibility to be injectable and even to be crosslinked in situ. Controversially, hydrogels that employ only DA crosslinking, still show some instability and rather slow gelation kinetics, which has led to their combination with other crosslinking methods (dual-crosslinking) [89], [103].

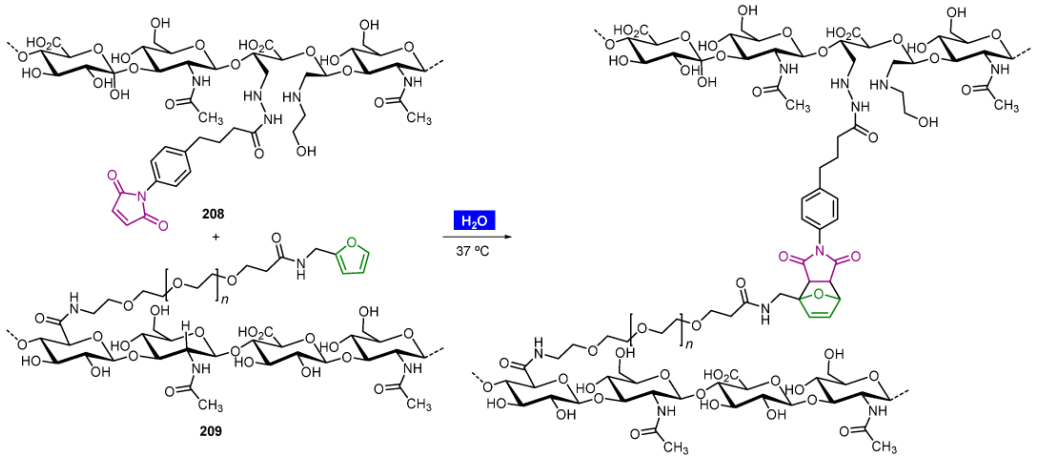

Figure 8 - An example of the Diels-Alder reaction between maleimide- and furan-functionalized polysaccharide precursors (hyaluronic acid) in an aqueous medium, which occurred at 37°C [106].

2.3.4. Mechanomodulatory hydrogels as versatile matrices to study fibroblast biology and promote wound healing

The mechanical microenvironment that surrounds cells has been recognized in recent years as having an important impact on the regulation of their behavior, not only in normal physiological processes but notably in wound healing and scar formation. Cells are constantly subjected to external and internal mechanical stimuli of varying magnitude, direction, and frequency, all of which elicit varied reactions from the cells. As stated, these forces are detected by the cells through mechanosensing, which are converted into biological signals (mechanotransduction) and trigger various signaling pathways [107]. Thus, substantial effort has lately been focused on understanding the influence of ECM mechanical properties in the context of wound healing towards investigating how cells perceive and transduce mechanical properties towards promoting skin regeneration.

Cunha et al demonstrated that by varying the amount of the crosslinking agent, the stiffness of the alginate/collagen-I hydrogels could be independently controlled without affecting other parameters, and the storage modulus was tuned from 50 to 1200 Pa. The dermal fibroblasts revealed considerable changes in cell shape immediately after being embedded in 3D hydrogels, with the cells spreading significantly more in soft hydrogels, but not in stiffer ones,

in which cells remained spherical. Tuning the storage modulus also resulted in various wound healing-related genetic profiles in dermal fibroblasts, with the varied expression of genes involved in inflammatory cascades, collagen production, surface adhesion receptors, and other ECM components. Thus, the inability of fibroblasts to spread directly influenced the downregulation of CCL2, an underlying mechanism of the chronic inflammatory response, the release of which is initiated by one of the FAKs signaling pathways [108]. Another research with poly(ethylene glycol) hydrogels focused on how varying the stress relaxation time influences the biological response of fibroblasts. This research revealed that hydrogels with faster stress-relaxation promoted the spreading and proliferation of fibroblasts embedded in 3D hydrogels. Moreover, they discovered that integrin-β1 is located at the periphery of these cells in hydrogels with a faster stress relaxation, however, as the stress-relaxation decreases, it is diffused throughout the cell. This behavior was attributed to the higher levels of FAKs in fibroblasts within the hydrogels with faster stress-relaxation time [109].

Most research results indicate that fibroblasts' potential to spread, differentiate, and proliferate is enhanced in soft viscoelastic materials, especially with higher stress-relaxation times (Table 3). Therefore, taking into consideration these studies, tuning the stiffness and viscoelastic properties of a dressing biomaterial might prove a powerful technique to modulate skin repair and regeneration. Wound dressing biomaterials that are applied to the wound site act as both a barrier and a scaffold, greatly impacting the cellular response. Their mechanical properties might possibly be adjusted to meet the appropriate stiffness to support and promote the regeneration of the wounded skin, and their design could even be altered to better adapt to the patient's demands. Furthermore, these biomaterials can be further improved with the combination of spatiotemporal control over the delivery of bioactive components, growth factors, or cells.

Table 2 - Research on the impact of mechanical properties of hydrogels on the biological response of fibroblasts.

Hydrogel	*Mechanical properties*	*Cells*	*Main findings*	*Refs.*
Alginate	Variation of stress-relaxation	3T3 Fibroblasts	Both cell spreading and proliferation were suppressed within materials with long timescales for stress-relaxation.	[110]
PEG	Variation of stress-relaxation	Porcine valvular interstitial cell	Higher levels of stress-relaxation induce cell spreading by day 1 and alignment by day 5. Key myofibroblast markers, including α-SMA and collagen 1, are significantly upregulated.	[111]
Alginate-PEG	Variation of stress-relaxation	3T3 fibroblasts	β1-integrin is in the periphery of the cell in the gels with fast stress relaxation, while it is diffusive throughout the cell in the gels with slow stress relaxation. Fast stress relaxation exhibited higher levels of phosphorylated FAK and paxillin.	[109]
PEG Thioester	Purely elastic vs. viscoelastic hydrogels (with elastic modulus of 1.4 kPa and stress relaxation or not)	3T3 fibroblasts	Viscoelastic substrates showed increased cell spreading and nuclear YAP/TAZ compared to purely elastic ones.	[112]
GelMA	Variation of the Young's modulus (from 49.9 ± 5.7 kPa to 139.1 ± 8.6 kPa)	hDF	Cell spreading and proliferation decreased with the increase of the young's modulus.	[113]
PEG-based	Variation of the elastic modulus (from 0.34 to 9.1 kPa)	hDF	The increase of polymer concentration and elastic modulus lead to a decrease in fibroblast spreading and proliferation.	[111]

Chapter 3 – Materials and Methods

3.1. Synthesis and characterization of Furan- and Maleimide-Functionalized Pectin-derived macromers

Pectin-based polymer (PectX) was used in this work as a non-cell interactive hydrogel matrix, allowing for tailored modification and biofunctionalization towards electing desired cellular responses. For the synthesis of either furan- (PectX-FUR) or maleimide-modified (PectX-MAL) pectin-based macromers, the polymer was firstly dissolved in ultrapure water (Milli Q) at 1 wt% while stirred at room temperature. After polymer dissolution, 4-(4,6-dimethoxy-1,3,5-triazine-2-yl)-4-methylmorpholinium chloride (DMTMM, Aldrich) previously dissolved in ultrapure water was added to the polymer at 1.519 g per g of PectX and left to react for 30 minutes, protected from the light to activate carboxylic groups in the polymer's backbone. Subsequently, either 5-methyl-2-furanmethanamine (98% purity, Thermo Scientific™) or 1-(2-aminoethyl) maleimide hydrochloride (Aldrich) were added to the polymer solution at 55.8 µl and 140 mg per g of PectX, respectively, and left react for 24 hours protected from light. Afterwards, the solutions were further diluted in ultrapure water, transferred to dialysis membranes (Spectra/Por® 3, SpectrumLabs), and purified against decreasing concentrations of sodium chloride (NaCl; AnalaR NORMAPUR® ACS) for 4 days. The solutions' pH was adjusted to 6.8–7.0 using sodium hydroxide (NaOH) and were filtered using 0.20 µm filter membranes (fisher brand). Finally, the solutions were frozen, lyophilized at -80°C and 0.008 mBar with the FreeZone 2.5 Plus freeze dryer (Labconco®), and stored at -20°C.

For ^{1}H Nuclear Magnetic Resonance (NMR) analysis, the modified polymer was dissolved in deuterium oxide (D_2O) at 13.3 mg/mL containing 5 µl of 3-(trimethylsilyl) propionic-2,2,3,3-d4 acid sodium salt (TSP-d4, Euriso-top), a standard solution. Then, samples were transferred to NMR tubes, which were taken for analysis to confirm the incorporation of either maleimides or furans into the pectin-based polymers. The NMR spectra not only allows the assessment of the polymer's functionalization but also allows the determination of the degree of substitution (DS) of both groups separately by comparing the integral values of the new peaks corresponding to protons of either furans (2.27 ppm) or maleimides (6.89 ppm) with a selected and unmodified proton on PectX backbone (4.00 ppm). In this way the DS was determined using Equations 1 and 2, respectively:

$$DS_{PectX-FUR}(\%) = \frac{Inetgral\ (2.27\ ppm)/_{3}}{Integral\ (4.00\ ppm)+Integral\ (2.27\ ppm)} \times 100 \quad (1)$$

$$DS_{PectX-MAL}(\%) = \frac{Inetgral\ (6.89\ ppm)/_{2}}{Integral\ (4.00\ ppm)+Integral\ (6.89\ ppm)} \times 100 \quad (2)$$

3.2. Fabrication of dual-crosslinked Pectin-based hydrogels

To produce the hydrogels, an appropriate mass of PectX-FUR and PectX-MAL was dissolved separately in Hank's Balanced Salt Solution (HBSS, Gibco) to prepare hydrogels at 2, 3 and 4% final polymer concentration (1:1 PectX-FUR to PectX-MAL ratio). Throughout the preparation of the hydrogels, the dissolved solutions were always placed on ice, maintaining them at a temperature of 4°C to prevent the Diels-Alder reaction between the maleimide and furan groups until the hydrogels were incubated. To the PectX-MAL solution, the cell-adhesive peptide CGGGGRGDSP (Genscript, cell-adhesive domain underlined) was added at desired concentration (0, 1, 2, and 4 mM) and left to react for 20 minutes. After this period, PectX-FUR was added to the solution, mixed and calcium chloride ($CaCl_2$; Acros Organics) was subsequently added at different concentrations (6, 8, 10, and 12 mM) and left to react for 1 hour. Then, 25 µl of the solution was pipetted onto a Teflon plate covered by a glass slide treated with Sigmacote (Sigma-Aldrich), to prevent hydrogel adhesion, separated by 1 mm spacers and incubated for 30 minutes at 37°C for thermal gelation.

3.3.Hydrogel characterization

3.3.1. Mechanical properties

To characterize the mechanical properties of the hydrogels, these were firstly soaked in complete Dulbecco's Modified Eagle's Medium (DMEM, Gibco) for 24 hours at 37°C. The samples were tested for both frequency sweeps (0.01 to 10 Hz at 1% strain) and strain sweeps (1 to 100% at 0.1 Hz), using a 4mm top plate and 8mm bottom plate of the Malvern's Kinexus Pro rheometer. Prior to testing, hydrogels were cut into samples with 4 mm of diameter to ensure sample standardization, and their height was measured using a picometer. Samples were loaded at a 20% compression was applied to ensure that the equipment plates had proper contact with the gels. Samples were tested at 37°C, and water droplets were added to the equipment's base plate to prevent dehydration.

3.3.2. Swelling ratio

To assess the swelling ratio of the 2, 3, and 4% polymer hydrogels, they were frozen immediately after preparation, then freeze-dried at -80°C, and finally weighed to determine their dry weight (W_D). Gels were then incubated in DMEM at 37°C for 24 hours, after which they were removed, the excess medium was extracted, and their wet weight was determined (W_S). The swelling ratio (Q) was calculated using Equation 3:

$$Swelling\ Ratio\ (Q) = \frac{W_S - W_D}{W_D} \qquad (3)$$

3.3.3. Degradation rate

The hydrogels were prepared, subsequently freeze-dried and prior to their incubation, their initial weight (W_I) was measured. Then the hydrogels were then left in a DMEM at 37°C and at certain time points, they were removed, washed with ultrapure water, frozen and lyophilized so that their final dry weight could be determined. The degradation rate is calculated by the percentage of weight loss through Equation 4:

$$Degradation\ (\%) = \frac{W_I - W_F}{W_F} \times 100 \qquad (4)$$

3.3.4. Gelation kinetics

To obtain the gelling curve of the hydrogels, the hydrogel precursor solutions were tested through an oscillatory time sweep performed in Malvern's Kinexus Pro rheometer where the strain and frequency are maintained throughout the assay at 1% and 0.1Hz, respectively. These were prepared as described above, with the exception of the addition of the $CaCl_2$ solution, which was only added immediately prior to the hydrogel solution being placed on the equipment base plate. The samples were tested at 37°C, and water droplets were added to the base plate of the equipment to prevent dehydration. Their elastic and viscous moduli were assessed over time, for both samples with and without the addition of $CaCl_2$.

3.3.5. Hydrogel treatment with EDTA

The removal of ionic crosslinks formed by the Ca^{2+} ions in PectX hydrogels was assessed. For this purpose, produced hydrogels with varying polymer concentrations were firstly incubated in DMEM for 24 hours. The hydrogels were then rinsed with HBSS before being incubated in EDTA solution at different concentrations (5, 10, 25, 50, and 100 mM) and their behavior was monitored throughout time.

3.4. Cell embedding in 3D hydrogels

To test the biological response of the hydrogels, human neonatal dermal fibroblasts (hNDFs) were incorporated into the hydrogels as individualized cells, to evaluate the impact of hydrogel properties on cell morphology and *de novo* deposition of ECM components. In addition, multicellular hNDF spheroids were fabricated and incubated in hydrogels to study how hydrogel properties impact the response of individual cells versus multicellular spheroids.

3.4.1. Cell source and maintenance

The hNDFs used in these experiments were thawed from -80°C and were used between passages 5 to 12 For this purpose, the cells were removed from the freezer, and 1ml of pre-warmed complete culture medium was added to their cryovial. The complete culture medium

was used in all experiments involving cells and is constituted by DMEM supplemented with 10% fetal bovine serum (FBS, Gibco), 1% antibiotics (100 U/mL penicillin and 100 µg/mL streptomycin, Corning®) and 1% amphotericin B (2.5 mg/L, Corning®). Next, the cells were cultured in cell culture flasks (SPL Life Sciences) with complete culture medium. In addition, the cells were incubated in 5% carbon dioxide (CO_2) at 37°C and used before reaching confluence.

In order to use the cells, they were previously trypsinized and counted, so that the number of cells necessary for the following experiments could be collected. To do this, the medium was removed from the culture flasks, and then the cells were washed with PBS. They were then incubated for 5 minutes at 37°C in a trypsin solution (Corning®), and after ensuring that the cells had detached from the bottom of the flask and were not in aggregates, complete culture medium was added to the solution to cease the trypsin's action. The cells were then collected in a falcon, several ups and downs were performed to ensure that there were no aggregates and that they did not settle to the bottom and the cells in suspension were counted using a Neubauer chamber. Finally, the required amount of cell suspension was removed and centrifuged at 1200 rpm for 5 minutes using the Eppendorf® Centrifuge 5804R, and the pellet is resuspended in the required quantity of medium/HBSS. Part of the cell suspension is also transferred to new culture flasks and incubated in the same way as explained above, with complete culture medium and at 5% CO_2 and 37°C.

3.4.2. Spheroids formation

To establish multicellular spheroids, the liquid overlay technique (LOT), using agarose as a non-adhesive surface, was the method used. As such, commercially available micro-molds (3D Petri Dish®, by MicroTissues, Inc.), with 81 circular recesses distributed in a 9x9 array, were used to make agarose molds, on top of which cells were seeded (Figure 9). Briefly, a sterile 0.9% NaCl solution was added to a previously sterilized in a dry cycle agarose powder (SeaKEM® LE Agarose, Lonza) to form a 2% agarose solution. Afterwards, the solution was heated until completely melted and filtered using a syringe and 0.20 µm membrane filters. It was then reheated using a dry heater, and 500 µL of the solution was added to the micro-molds to make 81-microwell molds. These were incubated at 37°C in DMEM for a minimum time of at least 1 hour, before being used to form the spheroids. The cells were trypsinized and centrifuged, and then the pellet was resuspended in 190 µl DMEM and added to the molds to obtain spheroids with 2500, 5000, and 10000 cells each. In order to ensure that the spheroids were formed, the molds were incubated in this manner for 30 minutes so that the cells could settle to the bottom in the mold, and only then was the culture medium added, and these were incubated in 5% CO_2 at 37°C.

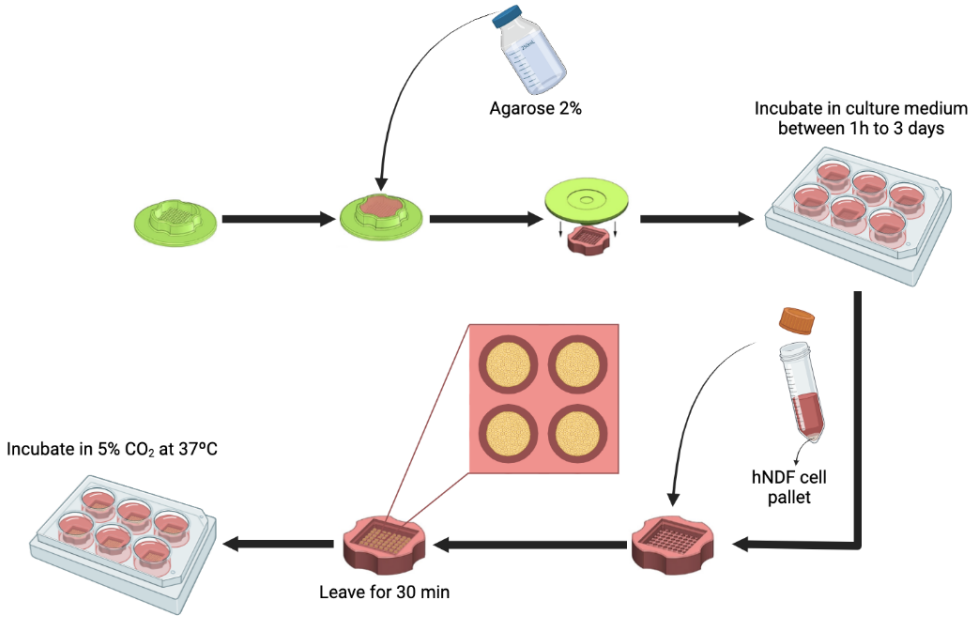

Figure 9 – Illustration of the procedure to prepare 3D spheroids made of human neonatal dermal fibroblasts. Created at biorender.com.

3.4.3. Cell embedding within hydrogels

To incorporate the individualized cells, hNDF were trypsinized and centrifuged as described above, and the pellet was resuspended in HBSS and added to the hydrogel solution before it was incubated at 37°C at final densities of either $2x10^6$ or $10x10^6$ cells/mL, corresponding to 8% of the final hydrogel volume. Next, 25 µL of the hydrogel solution with cells was pipetted onto a Teflon plate and incubated at 4°C for 30 minutes, after which the hydrogels were incubated in culture medium at 5% CO_2 and 37°C.

In the case of the 3D spheroids, they were removed from the molds at predefined time points using the culture medium in which they were incubated to gently push them out of the mold. These were then collected from the wells using a 1000 µL pipette tip so as not to tear them apart and passed into an eppendorf, and the culture medium was subsequently removed. The hydrogel solution was added to the spheroids, and they were carefully homogenized in it. Then, as performed for the individualized cells, 25 µL of the solution were dispensed into a Teflon plate and incubated at 37°C for 30 minutes, after which the hydrogels were incubated in culture medium at 5% CO_2 and 37°C.

3.5. Evaluation of cellular response within 3D hydrogels

3.5.1. Resazurin Assay

The metabolic activity for both the cells embedded in hydrogels and the spheroids in the 81 microwell molds was evaluated using the resazurin assay, at specific timepoints. Briefly, for

cell-laden hydrogels on days 1, 7, and 14, the hydrogels were incubated in a 20% of resazurin solution (v/v) (Sigma) that was added to each well for 2h at 37°C protected from light. After this period of time, 100 µl of medium were removed from the wells and transferred to a black-walled clear-bottom 96-well plate (Corning® Costar) in duplicates. Similarly, for the spheroids at days 1, 3, and 7 after cell seeding, the medium was removed from each mold and 2 mL of culture media containing 20% of resazurin solution (v/v) was added to each well. The samples were also incubated for 2 hours at 37°C in the dark, after which, 200 µL of medium from each condition was transferred to the black-walled, clear-bottom 96-well plate, in triplicates. Finally, the fluorescence of all samples was measured at the excitation and emission wavelengths of 530 nm and 590 nm, respectively, using SynergyMx™ MultiMode Microplate Reader (BioTek™). After the data was analyzed and the metabolic activity values were normalized to day 1.

3.5.2.Spheroid Characterization

The spheroids were characterized by evaluating their dimensions at specific time periods of their maturation. For this purpose, the spheroids were examined and imaged through 4x and 10x objectives of a microscope, the EVOS™ XL Core Imaging System (Invitrogen™). The pictures were later processed using Fiji (ImageJ), which allowed the measurement of the spheroids.

3.5.3. Cell Viability (Live/Dead assay)

Cell viability was also determined using the Live/Dead assay on hydrogels containing individualized cells at a density of $10x10^6$ cells/ml at day 14. For this assay, the hydrogel samples were firstly washed in HBSS incubated for 5 minutes in 5% CO_2 at 37°C and then washed 3 consecutive times in unsupplemented DMEM without phenol red. Following this, the hydrogels were incubated in DMEM containing Calcein AM and Ethidium homodimer-1, which stain the live and dead cells, respectively, for 30 minutes at 37 °C. A DMEM solution was prepared with 0.24% (v/v) Calcein AM and another with 0.20% (v/v) Ethidium homodimer-1, which stain living and dead cells, respectively, and then these were mixed (1:1). Next, the hydrogels were incubated in this solution for 30 minutes at 37°C and then washed in HBSS and incubated for 5 minutes with 5% CO2 at 37°C. Finally, the samples were incubated under these same conditions in DMEM without phenol red and analyzed using a confocal laser scanning microscope (Leica TCS-SP5, Leica Microsystems).

3.5.4. Cell Morphology and ECM deposition

The cell's morphology and the deposition of ECM molecules deposition were observed by the staining for F-actin and nuclei, as well as fibronectin or collagen type-I, so at specific timepoints, the cell/spheroid-laden hydrogels had to be fixed. To do this, the incubated

samples were washed with HBSS, fixed with a 4% (v/v) paraformaldehyde (PFA, Electron Microscope Sciences) in HBSS for 20 minutes, washed 3 consecutive times in HBSS to finally be stored in HBSS at 4°C. Prior to the staining of the cells, they were permeabilized with Triton X-100 0.1 (v/v)% in HBSS for 10 minutes at room temperature, and then the samples were washed 3 times with HBSS. To observe the cell's morphology only, the samples were incubated in an HBSS solution containing Alexa Fluor® 488 Phalloidin (Invitrogen™ - Thermo Fisher Scientific) (1:80) and 4',6-diamidino-2-phenylindole (DAPI; Vector Labs) (1:3000), for the staining of the F-actin and nuclei, respectively. Initially, it was left for 45 minutes at room temperature under agitation and then transferred to 4°C overnight while maintaining the agitation. Finally, the samples were washed 3 times with HBSS and stored at 4°C protected from the light in HBSS, until observed in CLSM. For the staining of the ECM components, after the samples were permeabilized and washed, they were also incubated with bovine serum albumin (BSA) 1% (v/v) in HBSS for 30 minutes at room temperature. Afterwards, the hydrogels were incubated in an HBSS solution with either rabbit anti-fibronectin (Sigma-Aldrich) (1:400) or rabbit anti-collagen type-I (Rockland) (1:200), Alexa Fluor 488 phalloidin (1:80) and DAPI (1:3000) and remained overnight at 4°C under agitation. Then, samples were washed 3 times with HBSS and incubated in HBSS with Alexa Fluor 594 goat anti-rabbit (Invitrogen™) (1:1000 fibronectin staining; 1:500 collagen staining) for 45 minutes at room temperature under agitation. Once again, the samples were washed 3 times with HBSS and stored at 4°C protected from the light in HBSS, until observed in CLSM.

3.6. Statistical Analysis

Statistical analyses were all performed using the GraphPad Prism 9 software and the results are presented as the mean ± standard deviation (SD). The non-parametric Mann–Whitney test was applied with 95 % confidence interval and statistically significant differences marked with $p < 0.05$ (*), $p < 0.01$ (**), $p < 0.001$ (***) and $p < 0.0001$ (****).

Chapter 4 - Results and Discussion

4.1. Synthesis and characterization of PectX-MAL and PectX-FUR macromers

In order to mimic key properties of the ECM, it is necessary to endow the hydrogel with specific features such as a viscoelastic behavior, and the ability to support cell adhesion and regulate tissue morphogenesis. Based on that, a dual-crosslinking strategy was employed to fine-tune the rheological and mechanical properties of the hydrogels, while a bioorthogonal Michael-addition reaction was used to tether cell-adhesive peptides into the gel network. Regarding the viscoelastic properties, ionic crosslinking was applied via a reaction of carboxylic groups in polymer backbone with calcium ions as it leads to the formation of physical hydrogels with greater capacity for energy dissipation and, therefore, contributing significantly to their viscoelasticity. Although several divalent cations could be used for this physical crosslinking process, calcium chloride was used as the ionic crosslinker for these dual crosslinked hydrogels, since it has been widely explored for the crosslinking of alginate hydrogels owing to its high solubility, which results in faster gelation [97]. Additionally, ionic crosslinking is also a suitable method to adjust the rheological properties of hydrogels for future 3D bioprinting applications [92]. The ionic crosslinking using Ca^{2+} has been previously employed in the research group to crosslink pectin polymers, delivering interesting results regarding the printability of pre-crosslinked hydrogels, allowing the bioinks to flow through the nozzle and maintaining shape after deposition, as well as cellular response [114]. As it is well known, non-covalent crosslinks formed via physical crosslinking are often weaker and more prone to disruption when subjected to mechanical stresses than covalent bonds formed through chemical crosslinking. Thus, a chemical crosslinking approach based on the Diels-Alder reaction was also adopted to enhance the hydrogels' stability during culture and to modulate their mechanical properties. This reaction was selected to provide the hydrogel with dynamic covalent bonds that would offer it much of its deformation resistance (elastic behavior) by forming strong polymer chain-to-chain bonds. Moreover, it also occurs at physiological pH and temperature conditions without the formation of any by-products, which is advantageous for possible in situ crosslinking. The DA reaction commonly occurs between electron-rich dienes and electron-poor dienophiles. Among the several diene-dienophile combinations available to promote the DA reaction, the conjugation of furan with maleimide groups is one of the most explored, due to their faster reaction under physiological conditions. Furthermore, the use of a furan derivative containing a methyl group has recently been employed since it is more electron-rich than furan, allowing for further enhancement of gelation kinetics [83]. To enable the Diels-Alder reaction, the polymers had to be firstly functionalized with maleimide and furan groups. Furthermore, as the polymer does not contain cell adhesion sites, it was important to biofunctionalized the

hydrogels with relevant biochemical cues, such as the addition of cell adhesion peptide sequence accomplished via the thiol-Michael addition click chemistry. Employing all of these strategies we were able to modulate the hydrogel's mechanical and biological properties, evaluating the fibroblast's response both as individualized cells and multicellular spheroids.

To this end, PectX polymer was functionalized with either maleimide or furan groups to generate PectX-MAL and PectX-FUR macromers, which were subsequently used to dual crosslinked cell-loaded hydrogels through a combination of ionic gelation and Diels-Alder reaction. To accomplish this, the PectX polymer was firstly mixed with DMTMM, a reagent that allowed the activation of the carboxyl groups through esterification, forming a reactive triazine ester intermediate that then suffers nucleophilic substitution by an amine group, which is present in the maleimides and furans used, resulting in the formation of an amide bond [94] (Figure 10).

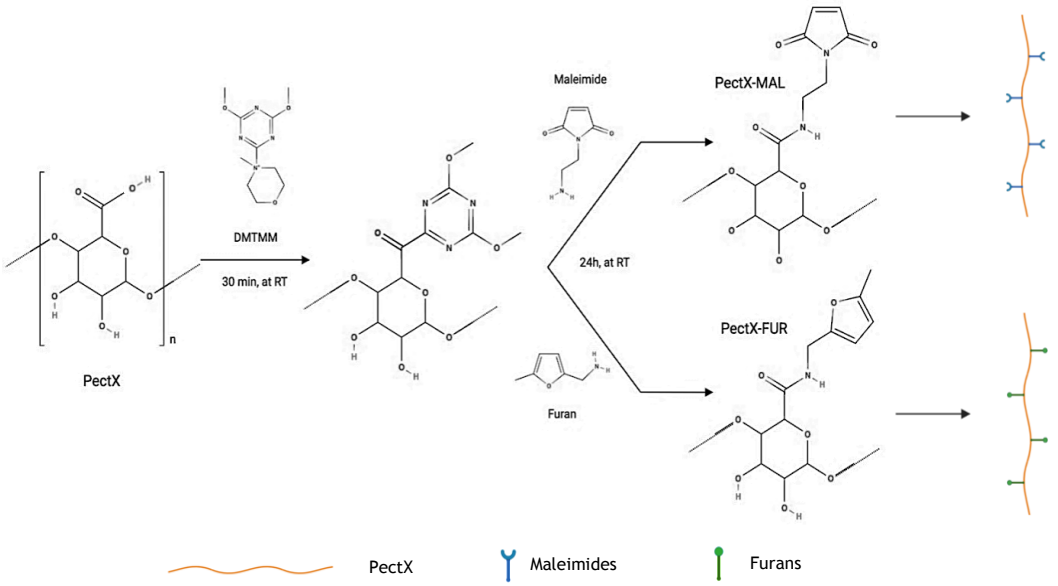

Figure 10 - PectX modification with maleimide and furan groups for the synthesis of PectX-MAL and PectX-FUR macromers. The DMTMM was added to the PectX polymer and left to react for 30 minutes at room temperature, activating the carboxyl groups. Then, 1-(2-aminoethyl) maleimide hydrochloride (a) or 5-methyl-2-furanmethanamine (b) were added separately, leading to PectX-MAL and PectX-FUR.

The incorporation of maleimide and furan groups to the polymer chains was confirmed through the use of ^{1}H NMR analysis, where distinctive new peaks of these groups were identified and were previously absent from the of pure PectX spectrum. The analysis of the ^{1}H NMR spectra, as seen in Figure 11, reveals the appearance of a peak at 6.89 ppm in PectX-MAL, which is attributed to maleimide groups, while in the PectX-FUR there is a noticeable peak at 2.27 ppm, indicating the presence of the furan groups. When comparing these two spectra to the PectX spectrum, it is possible to perceive that these peaks were not present at all in pure PectX, confirming the successful functionalization of the newly synthesized polymers. In

addition, through the analysis of the NMR spectra, it was also possible to determine the degree of substitution for each modified polymer. This was done by comparing the integrals of either the methyl group (-CH_3, three protons) of the furans (2.27 ppm) or the carbon double bond (two protons) of the maleimides (6.89 ppm) to a known and unmodified proton on the backbone of the PectX polymer (4.00 ppm) according to the Equation 1. Thus, DS values of 7.08 ± 0.29% and 8.51 ± 0.21% were obtained for the functionalization with furans and maleimides, respectively. The reproducibility and control over the reaction conditions were confirmed by repeating the modification of this polymer with both groups, and very similar integral values were obtained (Supplementary Figure S1).

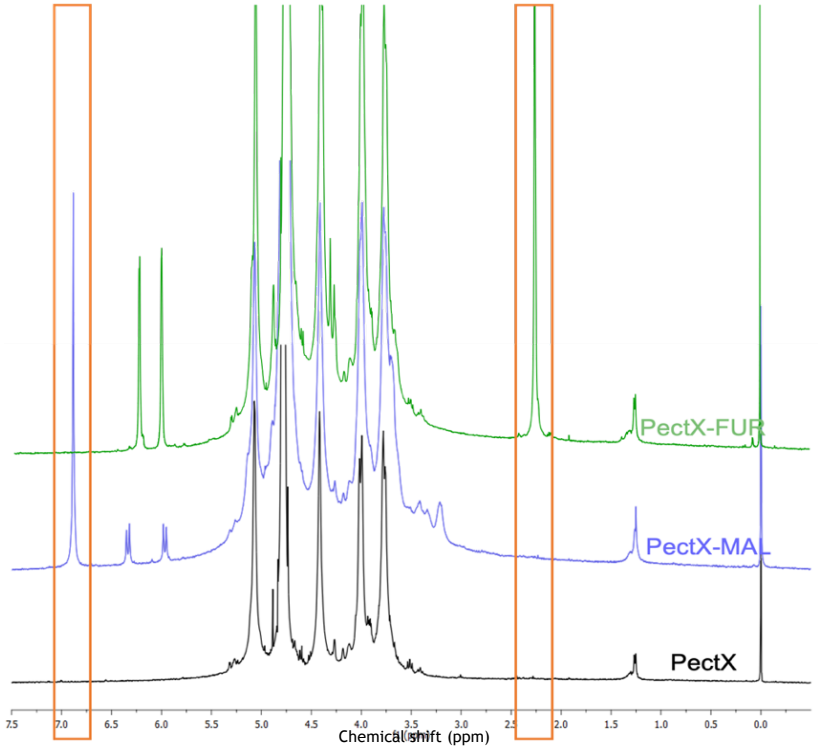

Figure 11 - ^{1}H NMR spectra (D_2O, 400MHz) of pure PectX, PectX-MAL, and PectX-FUR, after its functionalization with maleimide and furan groups. New peaks are visible in the spectra of PectX-MAL and PectX-FUR that are not found in the spectrum of pure PectX, with the maleimides peak at 6.89 ppm and the furans peak at 2.27 ppm.

4.2. Hydrogel preparation and characterization

The dual crosslinked hydrogels were prepared as illustrated in Figure 12 using different final polymer concentrations (2%, 3%, and 4%), but keeping fixed the ratio between PectX-MAL and PectX-FUR (1:1). The final polymer concentration of hydrogels was varied to understand how it influences the physical properties of the hydrogels and, later, how this affects cellular response, since varying this parameter also affects the number of available sites for the DA

crosslinking reaction. As PectX lacks cell adhesion sites in the polymer's backbone, a cell-adhesive peptide sequence (CGGGGRGDSP, cell-adhesive domain underlined) was also incorporated into the hydrogel, enabling integrin-mediated cell adhesion and cell-matrix communication, and conferring the hydrogel with properties that resemble this feature of the cell's native environment. The cell adhesive peptide was added to the PectX-MAL at a final concentration of 0, 1, 2, or 4 mM, in order to compare its impact on cells response and determine its optimal concentration. After the reaction of the cell adhesive peptide with the maleimide groups, PectX-FUR was added to the solution and subsequently, $CaCl_2$ was also added to the solution. The solution was kept at 4°C, inhibiting the temperature-dependent DA reaction between the maleimide and furan groups and enabling the ionic crosslinking process to proceed first. This crosslinking happens between the carboxyl groups in PectX, which ionize when in contact with the aqueous media, allowing them to react with the Ca^{2+} in the $CaCl_2$ solution. Calcium chloride was also added at different concentrations (6, 8, 10, and 12 mM) to evaluate the ionic crosslinking effect both on the hydrogel's mechanical properties and the cell's behavior.

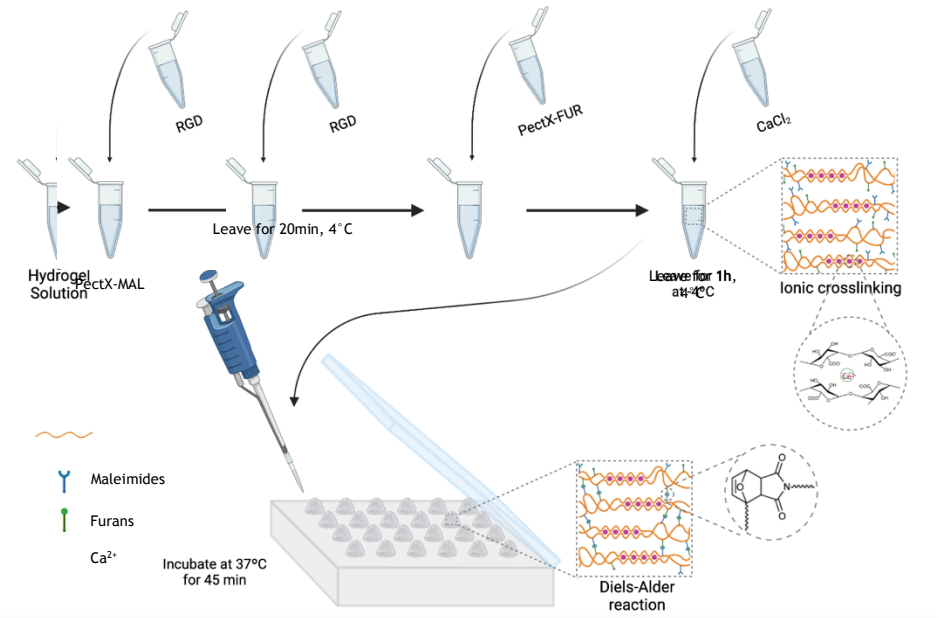

Figure 12 - Schematic illustration of the preparation of dual-crosslinked hydrogels. To create the hydrogels, a previously dissolved solution of PectX-MAL containing the maleimide groups was mixed with a solution containing an RGD peptide which promotes cell adhesion. The solution of PectX-FUR, which includes the furan groups, was then added, followed by a solution containing Ca^{2+} ions, promoting the ionic gelation between the carboxyl groups. Finally, the solution was incubated at 37°C to promote the Diels-Alder reaction between the maleimide and furan groups, leading to the formation of dual crosslinked hydrogels.

In order to understand how the mechanical properties of the cell microenvironment influence cell response, the hydrogels used for this purpose must be tailored with elastic and viscous moduli values similar to those of the target tissue, which in this research work is the healthy skin. The rheological properties of developed hydrogels can be adjusted through several strategies, such as changing the final polymer concentration, the concentration of the crosslinking agent ($CaCl_2$), the ratio between maleimides to furan groups, and even the degree of substitution of the functional groups incorporated in the polymer backbone. As previously mentioned, increasing the polymer concentration will also lead to an increased density of furan/maleimide groups present in the solution, resulting in a superior crosslinking degree via DA crosslinking reaction. Additionally, increasing the $CaCl_2$ content for the ionic gelation would also result in the alteration of the mechanical properties of the hydrogels as well as in the ratio between physical to covalent crosslinks in the gel network. Thus, in both strategies a change in the degree of crosslinking can be observed, resulting in modulation of the overall mechanical properties of the hydrogels and in the alteration of the types of bonds present in the gels, which ultimately could impact cell response, namely their morphology, proliferation, differentiation, and matrix deposition.

To evaluate how polymer concentration impacts the mechanical properties of hydrogels, dual crosslinked gel networks were synthesized using a final polymer content of 2, 3, and 4%, while maintaining the $CaCl_2$ and RGD concentration at 10 and 2 mM, respectively. In addition, gels were also prepared using different concentrations of CaCl2 (6, 8, 10, and 12 mM), while fixing the final polymer concentration at 2% and RGD at 2 mM. These different hydrogels were subjected to frequency and strain sweep assays (Figure 13A and D), to determine their elastic (G') and viscous (G") modulus. Overall, both strategies were suited to tune the mechanical properties of hydrogels, though varying the polymer concentration proved to be more effective. In this way, through the variation of the polymer concentration, it was possible to modulate the elastic moduli values between 1528.31 ± 297.80 and 3898.99 ± 4863.01 Pa and of viscous moduli between 193.51 ± 73.30 and 461.01 ± 111.76 Pa (Figure 13B and C). On the other hand, although these values also differed with the concentration of Ca^{2+}, this difference was not as significant, with the elastic moduli values ranging from 921.40 ± 260.60 to 1699.73 ± 50.03 Pa and those of viscous from 130.09 ± 42.07 and 230.08 ± 95.22 Pa (Figure 13E and F). Previously we had seen that the values of the elastic and viscous moduli varied with their measurement with and without the epidermis, with the full-thickness skin having values of G' between 325.0 and 1227.9 Pa and of G" between 68.5 and 189.9 Pa and the dermis only having higher values with the G' ranged between 434.9 and 6620 Pa and those of G" between 126.3 and 458.6 Pa. Comparing these values with the results obtained by varying the concentration of the ionic crosslinking agent and polymer in the hydrogels we were able to modulate the elastic and viscous modulus within the range of the healthy dermis and some vales were also attained in the full-thickness skin interval. These findings show that the degree of crosslinking can be

tuned by varying both the polymer concentration and the $CaCl_2$ concentration. However, the polymer concentration proved to be a more efficient strategy in modulating both the elastic and viscous properties, since, as previously stated, the Diels-Alder reaction between the maleimide and furan groups provides dynamic covalent bonds between the polymers chains that not only have the strength of covalent bonds but are also reversible like physical crosslinks. Although the reversibility of these covalent bonds has been established at higher temperatures, this behavior at physiological temperatures is still not well known. On the other hand, ionic crosslinking, as most physical crosslinks, present a reversible behavior, the bonds generated by this approach are much weaker which limits the extent of the modulation of the hydrogels' mechanical properties, as their bonds are more easily disrupted.

The gelation profile of the hydrogels was assessed using an oscillatory time sweep, which allows for the observation of the crossover point between the modules, indicating the reaction kinetics (Figure 13G). In this case, the crossover occurs almost instantaneously after $CaCl_2$ addition due to the fast reaction of ionic gelation. In addition, it is also noticeable that the mechanical properties of hydrogels in both conditions remained stable after 1 hour since there are no significant variations in the values of G' and G". At 1h of gelation, the mechanical properties of hydrogels were 1100 ± 494.97 and 58,56 ± 23.45 Pa for samples with the $CaCl_2$ addition and 2.19 ± 1.64 Pa and 88.88 ± 0.61 Pa for samples without the addition of the ionic crosslinker. The swelling behavior of the hydrogels is intimately related to their crosslinking degree, as an increased crosslinking degree leads to the formation of denser gel networks. Therefore, lyophilized hydrogels were weighed and then incubated for 24 hours in culture medium before being weighed once again. The swelling rate was determined (Figure 13H) and demonstrated, as expected, that with the increase of polymer and consequently of the degree of chemical crosslinking, a decrease in the swelling of the hydrogels is observed. The degradation rate of hydrogels incubated in DMEM for 7 days was also assessed (Figure 13I), and as expected, the hydrogels exhibited minimal degradation with a similar profile between them. Such mass loss can be attributed to the sol fraction of the gels, though quantification of sol-gel conversion is required to confirm this hypothesis. Chelsea et al. reported that adjusting the crosslinking density in hyaluronic acid hydrogels crosslinked by DA reaction between furan and maleimide groups did not significantly affect the mass loss when these gels were incubated in PBS alone and that the only factor leading to degradation had been the presence of the hyaluronidase, which did not target the DA bonds but the polymer itself. Furthermore, it was also reported in this study that the crosslinking density present in the hydrogels has a significant impact on gel swelling, with the increase in furan maleimide ratio resulting in the decrease of the hydrogels swelling [115].

Furthermore, to evaluate if the amount of RGD incorporated in the hydrogels was dependent on either the peptide content or the polymer concentration, the peptide's grafted percentage was determined after its incorporation (Figure S2). Results demonstrated that by

fixing the polymer concentration at 2%, increasing the initial RGD concentration from 1 to 2 mM does not result in significant differences in the final density of grafted RGD. Additionally, the results were similar when maintaining RGD concentration at 2 mM and varying the polymer concentration between 2 and 4%. Overall, the percentage of RGD incorporated in the hydrogels ranged between 81.24 ± 1.36% and 85.63 ± 0.38%, indicating the efficiency of the click Michael-addition reaction.

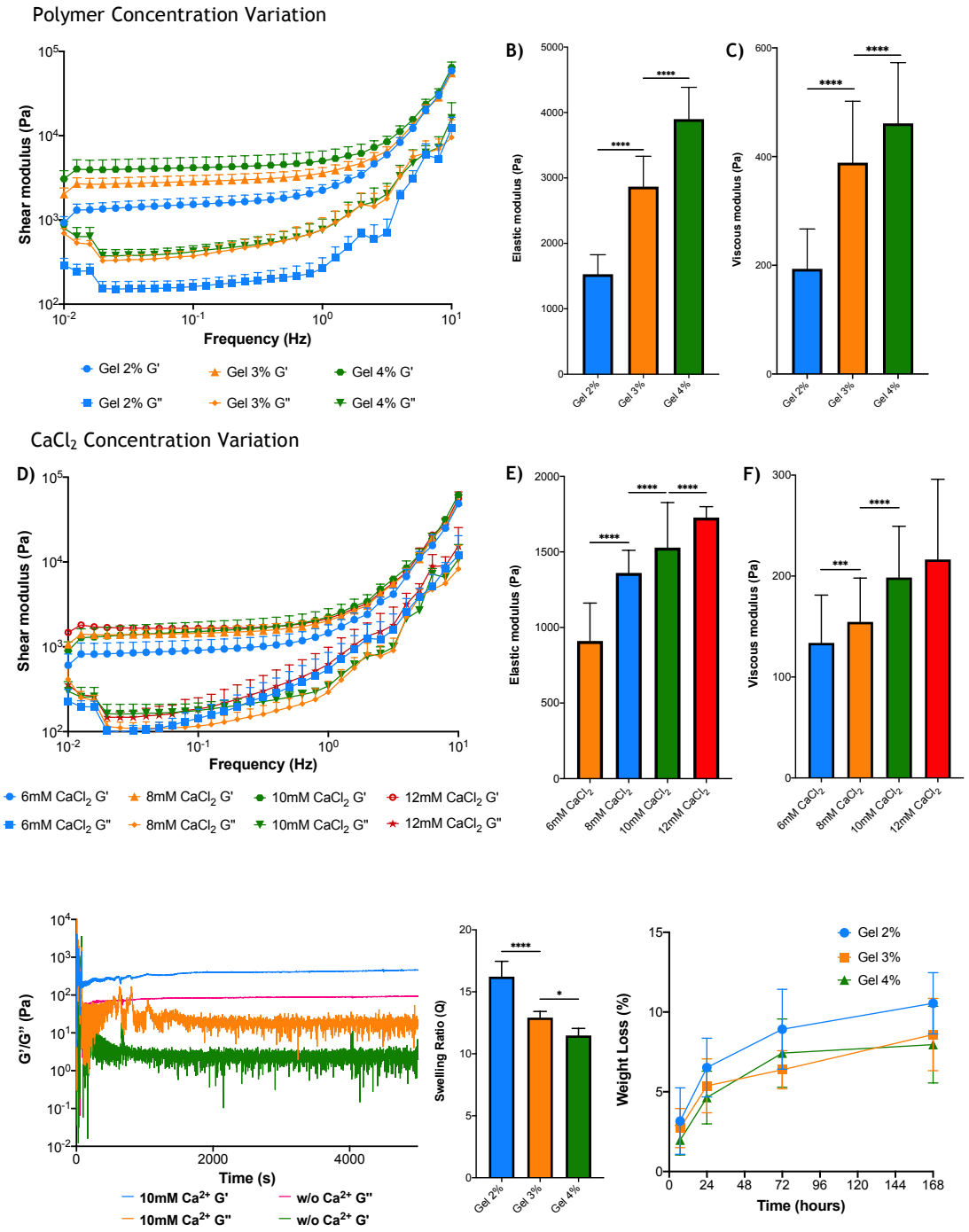

Figure 13 – Physical properties of dual crosslinked PectX hydrogels prepared with different concentrations of polymer and $CaCl_2$. **(A)** Storage (G') and loss (G'') moduli of hydrogels with 2, 3,

and 4% polymer final concentrations via frequency sweep assays. Elastic moduli **(B)** and viscous moduli **(C)** of hydrogels with different polymer concentrations, fixing $CaCl_2$ and RGD at 10 and 2 mM. **(D)** Storage (G') and loss (G'') moduli of hydrogels with 6, 8, 10, and 12 mM Ca^{2+} crosslinking agent concentrations via frequency sweeps assays. Elastic modulus **(E)** and viscous modulus (F) of hydrogels with different crosslinking agent concentrations. **(G)** Gelation time of the hydrogels with and without Ca^{2+} crosslinking hydrogels with the evolution of elastic (G') and viscous (G") moduli as a function of time at 37°C. **(H)** Swelling ratio of hydrogels with different polymer concentrations upon incubation in supplemented DMEM for 24h. **(I)** Degradation rate of hydrogels prepared with different polymer concentrations, while maintaining $CaCl_2$ and RGD at 10 and 2 mM, over the course of 7 days. In all assays, the RGD concentration was fixed at 2 mM. ($p < 0.001$ (***) and $p < 0.0001$ (****))

Despite the fact that the hydrogel displayed minimal mass loss over the 7-day period, a chelating agent can be used to remove calcium ions from the gel network which leads to a significant reduction of the crosslinking degree with consequent release of entrapped compounds. EDTA is an aminopolycarboxylic acid that has been employed as a chelating agent since it can bind to ions such as calcium, disrupting the physical cross-links in hydrogels. Hydrogel de-crosslinking may be beneficial not only for further research regarding the embedded cells but also to promote a controlled hydrogel dissolution *in situ*. Indeed, this can be useful for the use of hydrogels as dressings for wound regeneration, where the application of a cell-compatible chelating agent at a suited concentration can be explored for painless hydrogel removal and wound bed cleansing. The de-crosslinking effectiveness of PectX hydrogels containing varying percentages of polymer and maintaining $CaCl_2$ and RGD concentrations at 10mM and 2 mM, respectively, was determined by immersing them in EDTA solutions of different concentrations (5, 10, 25, 50, and 100 mM) and qualitatively observing their behavior at different incubation times (10s, 30s, 60s, 5min and 10 min). The visual assessment (Figure 14) revealed that at a low EDTA concentration (5 mM), none of the hydrogels showed significant alterations after 10 minutes. However, when the solution concentration was increased, the de-crosslinking action became more prominent. The 2% polymer gels began to change shape after only 60 seconds in 10 mM EDTA solution and were almost dissolved after 10 minutes of incubation. The 3 and 4% gels only showed significant changes after 5 minutes and 10 minutes of treatment, respectively, which can be explained by the increased degree of crosslinking of these hydrogels. The further increase of the EDTA concentration demonstrated an acceleration of the de-crosslinking process, thus, with the use of a 25 mM EDTA solution, the 2% polymer hydrogels showed a reduction in structural stability after 10 seconds of immersion and almost complete dissolution after 5 minutes. On the other hand, the 3 and 4% hydrogels took longer to completely dissolve, requiring about 10 min of treatment, which could be related to the presence of chemical bonds in the gel network, which are not sensitive to the action of EDTA. In this case, the stability of the gel network is dictated by the balance between the water penetration and the crosslinking degree of the network throughout time. In general,

increasing the concentration of the chelating agent allowed the acceleration of the de-crosslinking process of the hydrogels, since with the increase of its concentration there was a higher number of molecules for the binding of the calcium ions, however, at high concentrations EDTA it could become cytotoxic to the cells.

As stated, EDTA is a chelating agent that rapidly sequesters divalent ions and has been frequently used to dissolve hydrogels. This compound has been widely employed in hydrogels containing alginate and calcium ions, which display physical crosslinking comparable to that observed when calcium ions are combined with pectin, both resulting in the formation of the egg-box model. Bidarra et al. employed this technique to recover human umbilical vein endothelial cells contained in RGD-modified alginate hydrogels by immersing them in a 50 mM EDTA solution for 5 minutes. The hydrogel was completely dissolved, and the cells were retrieved successfully. Furthermore, a cell viability assay revealed that cells in RGD-modified alginate hydrogels retained 80% vitality even after being exposed to the chelating solution [116]. Another work, aimed at assessing cardiac fibroblast release from alginate hydrogels also functionalized with an RGD peptide, investigated if the exposure to the chelating agent impacted cell viability. In this way, fibroblast suspensions were incubated for 15 minutes in EDTA solutions of various concentrations (0.5, 5, 10, 25, and 50 mM). This study indicated that exposing fibroblasts to different EDTA solutions had almost no effect on their viability (81%), which was similar to fibroblasts attached and incubated in PBS alone (78.0%) or in trypsin-EDTA (89.3%) [117]. However, although there have been nearly no studies reporting the use of EDTA solutions for *in-situ* de-crosslinking of hydrogels applied in skin wounds, one study compared the use of normal saline and normal saline supplemented with EDTA at relatively lower concentrations (0.1 mM) for wound irrigation. It was reported that, at the tested concentration, EDTA did not cause additional toxic effects, did not interfere with the healing process and also demonstrated antibacterial properties [118]. In a preliminary approach, a screening was performed to assess if the encapsulation of the cells within the hydrogels impacted the de-crosslinking using an EDTA solution. Although the visual results were not recorded, de-crosslinking was attempted on cell-laden hydrogels with 2% polymer, 2 mM RGD, 10 mM CaCl2, and different cell concentrations ($2x10^6$ and $10x10^6$ cells/ml) after 7 days of culture. The highest concentration of EDTA (50mM) was used in an attempt to dissolve the hydrogels and slightly more resistance to hydrogel dissolution was observed. Indeed, gels required about 10 minutes to completely dissolve compared to 5 minutes of cell-free hydrogels. Furthermore, this study was also performed on hydrogels incubated for a period of 14 days using a higher cell density (10x106 cells/ml). Results demonstrated that even after 25 minutes of exposure to EDTA solution at 50 mM the hydrogels still had not completely dissolved. This behavior can be attributed to the deposition of ECM components by the fibroblast cells, which makes it difficult to fully dissolve the network without the use of enzymes. However, further investigation is warranted to elucidate the impact of cell density and culture time on hydrogel de-crosslinking.

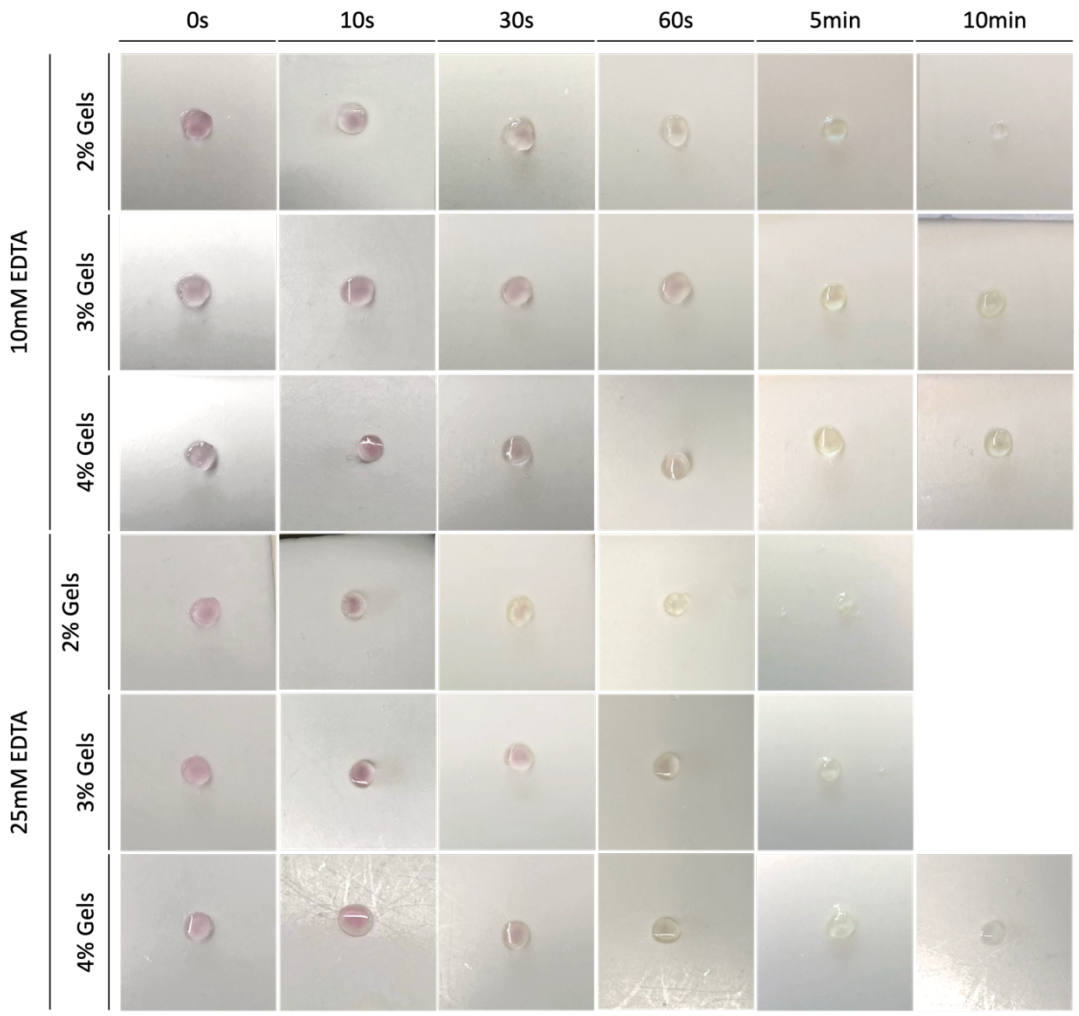

Figure 14 – Macroscopic images showing the impact of EDTA concentration and incubation time on the structural stability of cell-free dual-crosslinked hydrogels prepared with varying polymer content and 10 mM and 2mM of $CaCl_2$ and RGD, respectively.

4.3. Impact of hydrogel properties on the morphology and metabolic activity of fibroblasts in 3D

Since most cells, such as fibroblasts, have mechanosensors and therefore, are capable of perceiving and interpreting mechanical stimuli such as viscoelasticity and stiffness, it is critical for skin regeneration applications to develop a microenvironment capable of modulating their response in a manner that promotes regeneration while reducing or eliminating scar tissue formation. Furthermore, it is vital to understand how, and which cell fates are triggered when cells are embedded in 3D matrices with mechanical characteristics that either match or do not those of healthy skin. Indeed, some recent findings have shown matrix stiffness as a major driver of fibroblast activation and pro-fibrotic responses, which can lead to the development of hypertrophic or keloid scars [119]. In this way, the main objective of this work was to study how matrix stiffness impacts the cellular response of dermal fibroblasts in 3D towards the

rational design of hydrogel dressings capable of inducing the formation of healthy skin and supporting normal wound healing. Thus, hNDFs were selected for the cell studies as they act as mechanosensing cells that play a crucial role in dermal regeneration, particularly in the production and remodeling of extracellular matrix components. As previously stated, unmodified pectin-based polymers lack cell-adhesion sites. Therefore, an integrin-mediated cell adhesion peptide RGD had to be incorporated into the hydrogels. A study was conducted to understand how and to which extent the density of RGD tethered in the hydrogels influences the cells embedded in them. The initial peptide content was varied between 0 and 4 mM, while the polymer and $CaCl_2$ concentrations were kept constant at 2% and 10mM, respectively. The RGD impact was assessed through the quantification of the metabolic activity and assessment of the morphology of embedded cells by staining of the nucleus and cytoplasm, which was evaluated after 1 and 7 days of culture (Figure 15A and B). The hydrogels with concentrations of 1 and 2 mM of RGD peptide did not show significant differences in fibroblast morphology and metabolic activity of cells throughout the 7 days of culture. Indeed, only a slight increase in the metabolic activity of hydrogels with higher RGD concentration was noticeable. In both cases, fibroblast elongation was evident after only 24 hours of culture, with a considerable increase in metabolic activity by day 7 of culture. Furthermore, in hydrogels without the cell adhesive peptide (0 mM of RGD), the cells demonstrated no adherence to the matrix with a round morphology, which was predicted given the lack of cell adhesion sites in the hydrogel and also explaining the decline in metabolic activity between day 1 and 7 of culture. In the case of hydrogels containing 4 mM of RGD concentration, cells showed a highly spread morphology at day 7, but the increase in the metabolic activity was lower when compared to both 1 mM and 2 mM RGD-containing hydrogels. This behavior indicated that, while cells were able to elongate and adhere to the hydrogel, which was further exacerbated over the 7-day culture period, increasing the peptide concentration led to a reduction in their metabolic activity as they were probably overly attached to the matrix. These results suggest that the density of the peptide dictates the extent of cell spreading in 3D, which can be regulated simply by altering the concentration of RGD peptide added to the hydrogels. Thus, taking into consideration the results obtained both by CLSM imaging and metabolic activity measurements of the fibroblasts embedded within the dual crosslinked hydrogels, the 2 mM concentration of RGD appears to be optimal and, therefore, the remaining assays were performed with this concentration. The influence of this integrin-mediated cell adhesion ligand has been extensively researched and employed on hydrogels deficient in adhesion sites [106]. A study conducted by Pereira et al demonstrated in a similar way that fibroblast morphology was affected in an RGD concentration-dependent manner. The results through a Live/Dead assay showed that with RGD concentration between 0 to 2 mM cells remained alive for at least 7 days, however, demonstrated different morphologies. Fibroblasts cultured in RGD-free

hydrogels remained round throughout the experiment while in the presence of this peptide, they adhered to the matrix and elongated as a function of RGD's density [120].

As mentioned above, it is recognized that the mechanical properties of the wound environment have an effect on the healing process by regulating cell behavior [16]. Thus, to understand how the mechanical properties of the hydrogel affect cell response in terms of cell morphology and metabolic activity, these parameters were evaluated after the culture of hNDFs in hydrogels with different $CaCl_2$ or polymer concentrations. As we have seen, the reduction in the content of the ionic crosslinker leads to a reduction in the mechanical properties of the hydrogel, especially in the viscous modulus, since we now have a higher content of DA bonds that can lead to the network becoming more static. The reduction of the viscous properties of the gel led to fibroblasts showing a more rounded morphology, although after 7 days in culture they show some degree of cell sprouting. The 10 mM of $CaCl_2$ concentration proved to be the optimal condition of the physical crosslinking degree by promoting fibroblast adhesion and elongation, as well as an increase in their metabolic activity. However, the further increase in calcium chloride showed a reversal of this effect. Although cells were able to elongate within the hydrogel, the increase in the degree of crosslinking leads to an increase in cell confinement that could be associated with the reduction in their metabolic activity (Figure 15C and D). Furthermore, the study of the influence of the mechanical properties was also carried out by the variation of the polymer's concentration. The resazurin assay revealed a decrease in metabolic activity directly related to the increase in polymer concentration, and hence the mechanical properties of the hydrogels. This drop in metabolic activity is followed by a decrease in fibroblast spreading (Figure 15E and F). In 2% polymer hydrogels fibroblasts demonstrate an elongated morphology only after 24 hours of culture. On the other hand, hydrogels with 3 and 4% polymer demonstrate the opposite behavior, showing completely round after the first 24 hours. However, after this period of culture, in the 4% hydrogels, the cells remained completely round with only minimal sprouts, probably due to the increased confinement and decreased dynamics of the hydrogel, due to the greater amount of covalent bonds (DA). Taking all these results into account, in general, the concentrations of 2 mM RGD and 10 mM $CaCl_2$ have presented the most favorable results in the cell-laden hydrogels. Therefore, these were the concentrations selected for subsequent experiments.

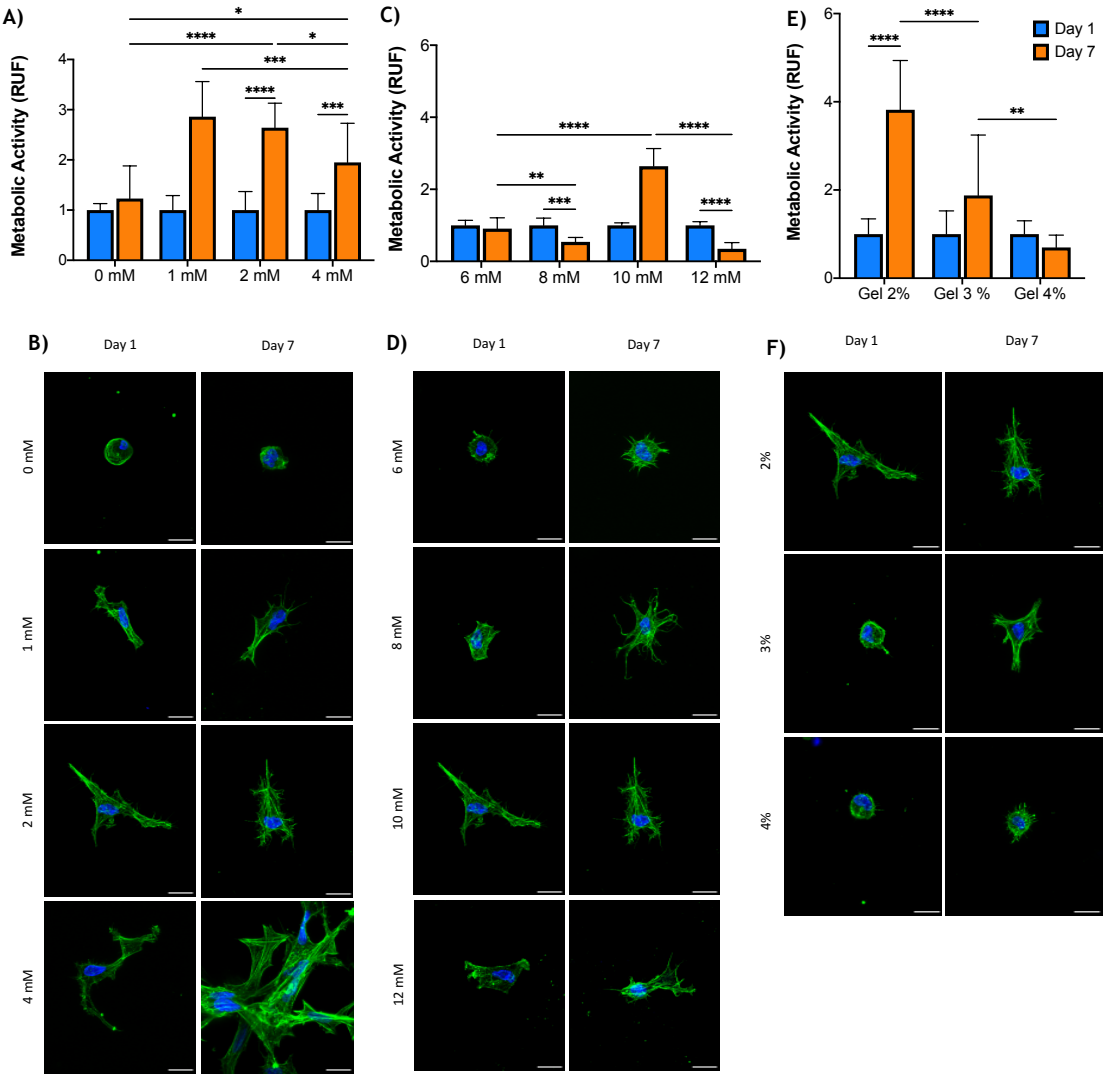

Figure 15 - Metabolic activity and morphology of dermal fibroblasts embedded within the dual crosslinked hydrogels throughout 7 days of culture. Cell metabolic activity measured through the resazurin assay on hydrogels with different concentrations of **(A)** polymer, **(C)** RGD peptide, and **(E)** calcium chloride. Cell morphology assessed through staining of the nucleus and cytoplasm on hydrogels with varying concentrations of **(B)** polymer, **(D)** RGD peptide, and **(F)** calcium chloride. (p < 0.01 (**) and p < 0.0001 (****); Scale bars: 20 µm)

4.4. Cell viability and matrix deposition in dual crosslinked hydrogels with different mechanical properties

To investigate how mechanical properties influence key cellular functions in the context of skin tissue engineering, such as the cell viability and deposition of ECM components, hNDFs were embedded in hydrogels with varying polymer concentrations at a higher cell density of 10x106 cells/ml and cultured for 14 days. A live/dead assay was performed on day 14 of culture (Figure 16A), showing that there were almost no dead cells and indicating the high

biocompatibility of hydrogels. Furthermore, the nucleus and cytoskeleton stained on days 1 and 14 of culture (Figure 16B), further corroborated the behavior previously observed in these gels using a lower cell density and allowing to observe if cells were able to communicate with each other forming multicellular networks. The cells embedded in the 2% gels were already elongated, forming interconnected cellular networks after only 1 day of culture, while the fibroblasts in the 3 and 4% polymer hydrogels remain spherical corroborating what was previously observed morphological behavior of cells embedded within hydrogels at a lower density. After 14 days in culture, in 2% polymer gels, cells maintained their dense interconnecting cellular networks and in 3% polymer hydrogels, with time, cells were able to exhibit a similar behavior also forming these networks. On the other hand, fibroblasts in 4% polymer hydrogels gels, even though they were capable of elongation and adherence to the matrix to some extent, there was no formation of these interconnecting cellular networks. This means that over time, cells are still cable of remodeling the matrix to some extent in order to form these multicellular networks, but this behavior is either stimulated or prevented by the matrix stiffness. Given that the hydrogels are not degradable, it is hypothesized that the mechanical compliance of the hydrogels along with the ability of the cells to locally rearrange the gel network are major determinants of cell response, i.e., spreading and morphology, in our hydrogels. Additionally, the metabolic activity of cells within these hydrogels was assessed (Figure 16D). In hydrogels containing 4% of polymer concentration, cells maintained their metabolic activity profile with a drastic decrease at day 7, however with a recovery of metabolic activity at day 14 to values close to the ones on the first day. Furthermore, cells within both the 2% and 3% hydrogels were able to increase their metabolic activity throughout the 14 days.

Fibronectin is a fibrous protein of the extracellular matrix of the vast majority of biological tissues, including the skin. It plays a key role in several important processes such as cell adhesion and migration and is also present in almost all stages of skin healing. Not only is it important for the formation of the fibrous clot after injury, but it has also been shown to be required for further deposition of other components of the ECM components essential for normal healing, such as collagen [121]. For this reason, fibronectin staining was also performed on day 14 (Figure 16C), and deposition of this ECM component across the hydrogel network was found on both the 2% and 3% gels, but more evident on the former. However, in the 4% gels, only minimal deposition of fibronectin was observed, which is only found in the periphery of the cells that are slightly more elongated. These observations could be attributed to the increased mechanical properties of hydrogels imparted by the chemical crosslinking that restrain the cells and reduce the ability of the cells to remodel the surrounding matrix towards spreading. A study performed on gelatin hydrogels produced via horseradish peroxidase (HRP)-catalyzed crosslinking, demonstrated that cell morphology, proliferation, and matrix components deposition are dependent on matrix stiffness. To this end, gelatin-based hydrogels

were produced with two different stiffnesses (1.1 and 6.2 kPa) and human dermal fibroblasts were then embedded within the gels. The stiffer hydrogels demonstrated that cells had difficulty spreading throughout the 14-day culture period, exhibiting a round shape with some sprouts. Moreover, these hydrogels also downregulated the expression of important ECM components such as collagen-I and -III and also fibronectin, when compared to cells cultured on tissue culture plates. However, fibroblast present on the soft hydrogels even though they did not demonstrate improvement in matrix deposition compared to those cultured in tissue culture plates, they did show to be homogeneously spread and elongated throughout the hydrogel, forming interconnected cellular networks for cell-cell communication [122].

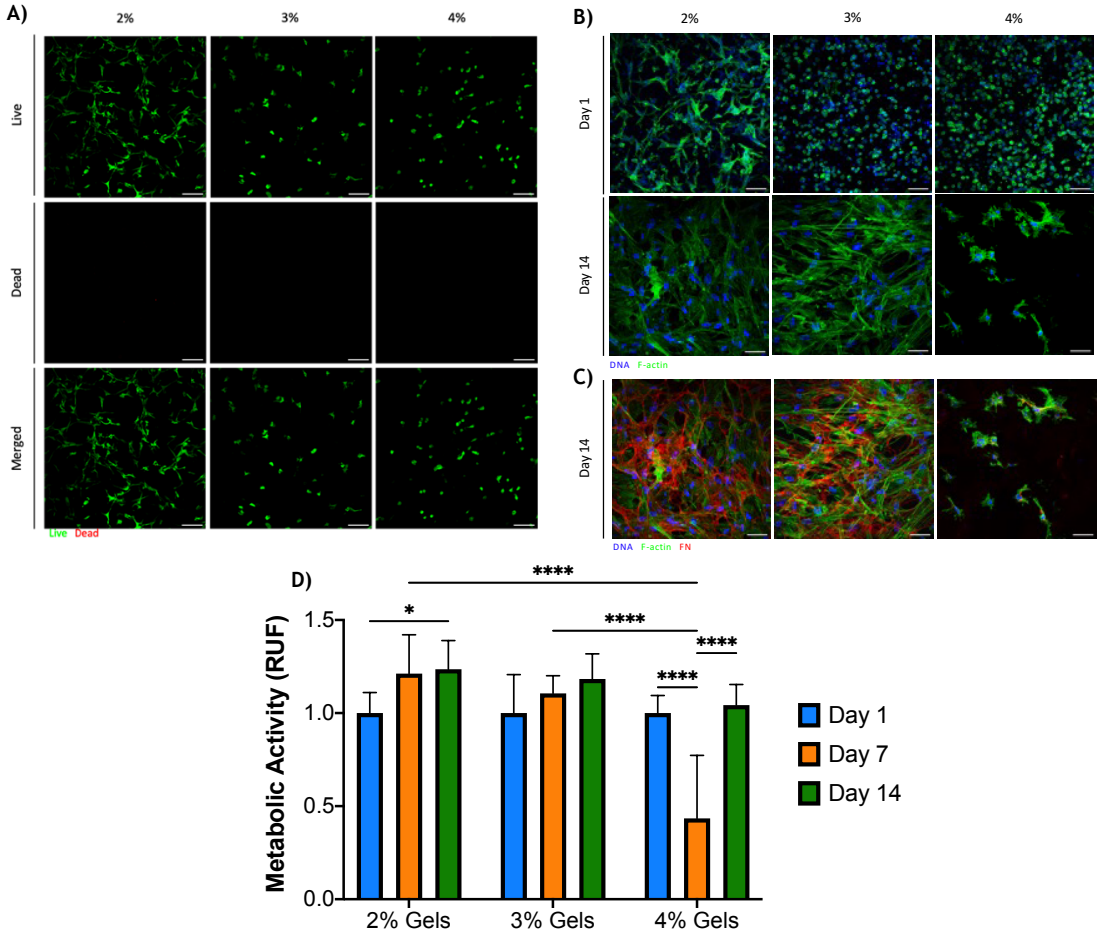

Figure 16 – Cell viability (A), morphology (B), matrix deposition (C), and metabolic activity (D) of fibroblasts embedded within hydrogels at different polymer concentrations, maintaining $CaCl_2$ and RGD concentrations at 10 and 2 mM. ($p < 0.05$ (*) and $p < 0.0001$ (****); Scale bar A and B (day 1): 100 µm; Scale bar B (day 14) and C: 50 µm)

4.5. Spheroids characterization and cell migration within the dual crosslinked hydrogels

The ability of cells to migrate within the hydrogel network is an important feature for the colonization of the hydrogels and also the production of ECM components, which are crucial in the context of skin regeneration. To assess and characterize cell migration in hydrogels, cell tracking using cell live imaging is usually performed, however, this is a much more time-consuming and complex process. In this sense, to determine whether dual crosslinked hydrogels allowed cell migration and how this cell function is influenced by the stiffness of the hydrogels, we chose to incorporate cell spheroids with different characteristics into the hydrogels, thus being able to evaluate cell migration through invasion of the hydrogels. Multicellular spheroids are usually formed by intrinsic self-assembly of cells [123] which in this case was promoted by their seeding onto 81-microwell round bottom agarose molds.

The agarose 81-microwell molds previously prepared were seeded at different cell densities to obtain spheroids composed of 2500, 5000, or 10000 hNDFs cells each. During spheroid formation, it was possible to observe that initially, the cells gather themselves into fragile cellular aggregates through intercellular interactions. Over time, these aggregates mature into more round, well-defined, and resistant spherical cellular structures due to contractile forces generated by actin stress fibers. Thus, the longer the maturation time, the greater the compaction of the aggregates, generating a denser cell-cell network [123]. This maturation process can be observed in Figure 17A. Prior to the embedment of the spheroids into the hydrogels, these were firstly characterized regarding their metabolic activity and size in the agarose molds throughout a 7-day period of time. Microscopy observation revealed that after only 9 hours of the cell seeding onto the molds, spheroids with 10000 and 5000 cells had already taken on a more round and compact shape, enabling them to be manipulated. However, spheroids made of 2500 cells were still loose and disintegrated after attempting their removal from the mold. Furthermore, the spheroid's diameter was assessed while in the mold, revealing that the fibroblast has a greater compaction tendency in the first 24 hours, but still exhibit some size decrease throughout the culture time (Figure 17B). The metabolic activity of spheroids was directly affected by the variation of cell densities, which were measured using resazurin assay at 24, 72 (3 days), and 168 (7 days) hours (Figure 17C), with an increase in metabolic activity, observed throughout the 7-day spheroid culture when compared to day 1. This increase, however, was much more pronounced in spheroids with lower cell density, which can be explained by the fact that the higher density limit nutrition, oxygen, and metabolic waste exchange from the outermost layer to the spheroid's core and vice versa, which create a hypoxic environment to the inner cells, reducing their metabolic activity. Experimental work performed the formation of fibroblast spheroids in a similar way using agarose micro-molds to prepare them with different sizes and evaluate their impact. This study found that spheroids

larger than 400 µm induced apoptosis due to the hypoxia gradient felt towards the core of the spheroid. In addition, as in our work, they found an initial decline in the size of the spheroids, showing that they become denser and more compact, stabilizing after 5 days. In spheroid s below 300 µm in size, tests were also performed that showed that there were no signs of necrosis or apoptosis and that the fibroblasts maintained their proliferative phenotype [124].

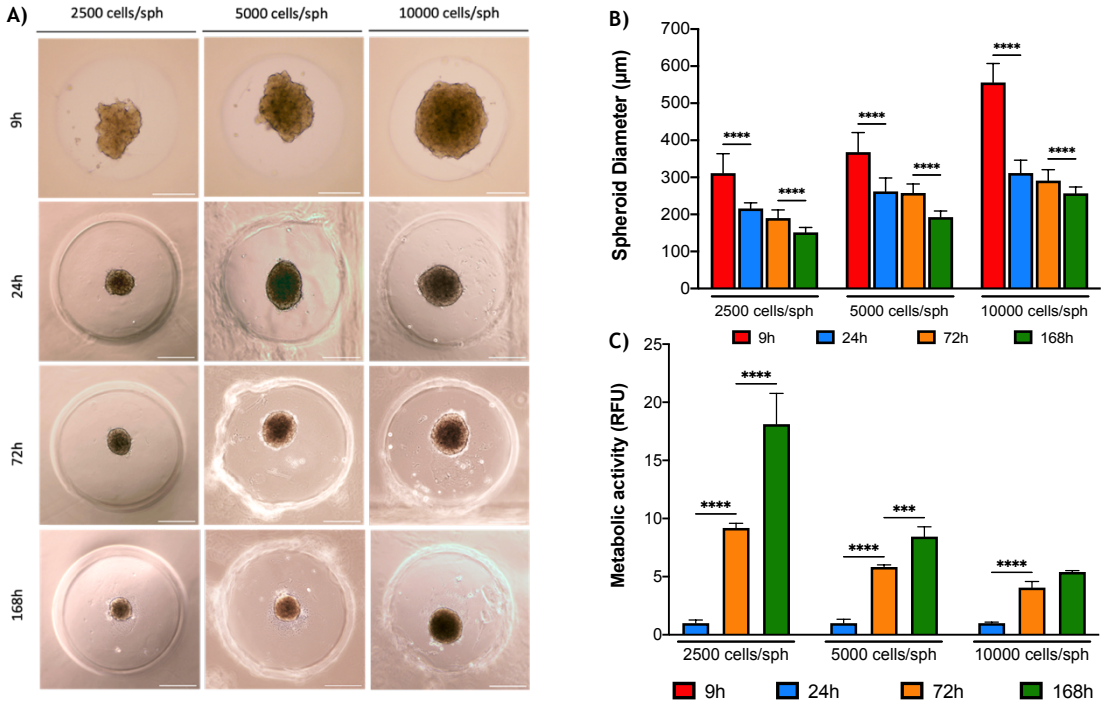

Figure 17 - Spheroid characterization. **(A)** Spheroid's diameter at different time points. **(B)** Spheroid microscopic imaging throughout the 7-day timeline. **(C)** Spheroid metabolic activity. ($p < 0.001$ (***) and $p < 0.0001$ (****); Scale bars: 250 µm)

After characterizing the formation of fibroblast spheroids, they were incorporated within the hydrogels (Figure 18A), and different parameters were compared to study their impact on fibroblast migration. In almost all experimental conditions some spreading of the cells was already visible at day 7 when observing the samples under EVOS™ microscopy. However, by day 14 these results were more pronounced, and a more accurate comparative analysis could be made. Thus, spheroids made of 5000 cells were incorporated with different maturation times (9 and 24 hours) in hydrogels of 2% polymer, 2 mM RGD and 10 mM $CaCl_2$. Through the images obtained by staining their cytoskeleton (Figure 18B), there were no significant differences between the conditions as both showed extremely elongated cells forming interconnecting cellular networks with a uniform spreading. In addition, in the image of the spheroid with a shorter maturation time, the core of the spheroid is quite visible, showing that fibroblasts are migrating throughout the hydrogels towards the colonization of the empty space.

In addition, the migration of cells from spheroids with different cell densities (2500, 5000, and 10000 cells per spheroid) with 24 hours of maturation was also studied by using hydrogels containing 2% polymer, 2mM RGD and 10mM $CaCl_2$ (Figure 18C). Compared to the 5000-cell spheroid described above, the spheroids with lower cell density showed total spreading of cells with no evidence of the pre-existence of a spheroid. Indeed, cells appeared to migrate randomly through the matrix, without the formation of cellular networks. However, this effect is possibly due to the reduced size of the spheroid and the smaller number of cells in it, allowing the spheroid to disassemble in a much faster manner increasing the migration distance between each other. In comparison, the spheroids with higher cell density did not show very significant differences from the spheroids with 5000 cells, and also demonstrated a high migration of cells that appeared elongated and forming interconnected cell networks. Although the distribution of these does not seem to be as uniform as in the spheroids with 5000 cells, due to the higher number of cells present.

Finally, the impact on the mechanical properties of the hydrogels was evaluated (Figure 18D). To do that, spheroids with 5000 cells each and 24 hours of maturation were incorporated into hydrogels with different concentrations of polymer (2, 3, and 4%), keeping the concentration of RGD and $CaCl_2$ fixed at 2mM and 10 mM, respectively. The 2% gels, as mentioned above, showed an increased migration capacity and the formation of dense interconnected cellular networks for cell-cell communication. However, this behavior was downregulated in the 3% gels and almost completely inhibited in the 4% gels. Through the cytoskeleton staining images, it is possible to observe that the 3% gels, after 14 days, although the cells were able to elongate, did not show large sprouts and migration beyond the spheroid's core. In hydrogels with 4% polymer, it is possible to observe that this behavior is similar, demonstrating even less cell elongation and migration in relation to the core of the spheroids. As previously shown through the use of individualized cells, the mechanical properties affect various behaviors of fibroblasts, and in this case, the increase in polymer concentration leads to a consequent increase in the crosslinking degree and, thus making the network denser and more static, confining the cells and inhibiting cell behaviors such as their elongation and migration.

To study the impact of the mechanical properties of hydrogels on multicellular spheroids, Kim et al. used GelMA hydrogels with varying polymer concentration to model their elastic modulus between 0.3 and 2.6 kPa and incorporated stem cells spheroid within the gels. Firstly, the density of spheroids in the hydrogels was evaluated to see if it could have any impact on cell migration. It was found that there were no significant differences in the cell sprouting area between high- and low-density hydrogels. Then, they proceeded to the characterization of the spheroids incorporated in the different gels. The gels with lower polymer densities and consequent lower elastic modulus demonstrate that the spheroids had higher cell sprouting and that this significantly decreased with increasing polymer concentration, with no differences

observed in stem cell spheroids within hydrogels with higher elastic modulus. Moreover, the spheroids within the different hydrogels were evaluated for apoptosis and proliferation using different staining's, and demonstrated that at higher polymer concentrations the cells exhibit a more apoptotic behavior due to hypoxia and spheroids within the more soft gels had grater proliferation rate [125]. In our work, the hydrogels with 3% polymer concentration have anelastic modulus comparable to those obtained at the highest polymer density in study of Kim et al. However, despite demonstrating that in stiffer gels there was no cell migration from the spheroids, contrary to what was observed in our hydrogels, they were only left in culture for a short period of time. Thus, the disparity of these results may be due to differences in the culture time of the spheroids, as well as in the viscoelastic properties of gels which were not characterized in this study and have been shown to significantly influence the ability of cells to migrate and remodel the surrounding ECM [125]. Overall, it was possible to unravel that using our hydrogel system, cell migration is mostly dictated by the polymer concentration.

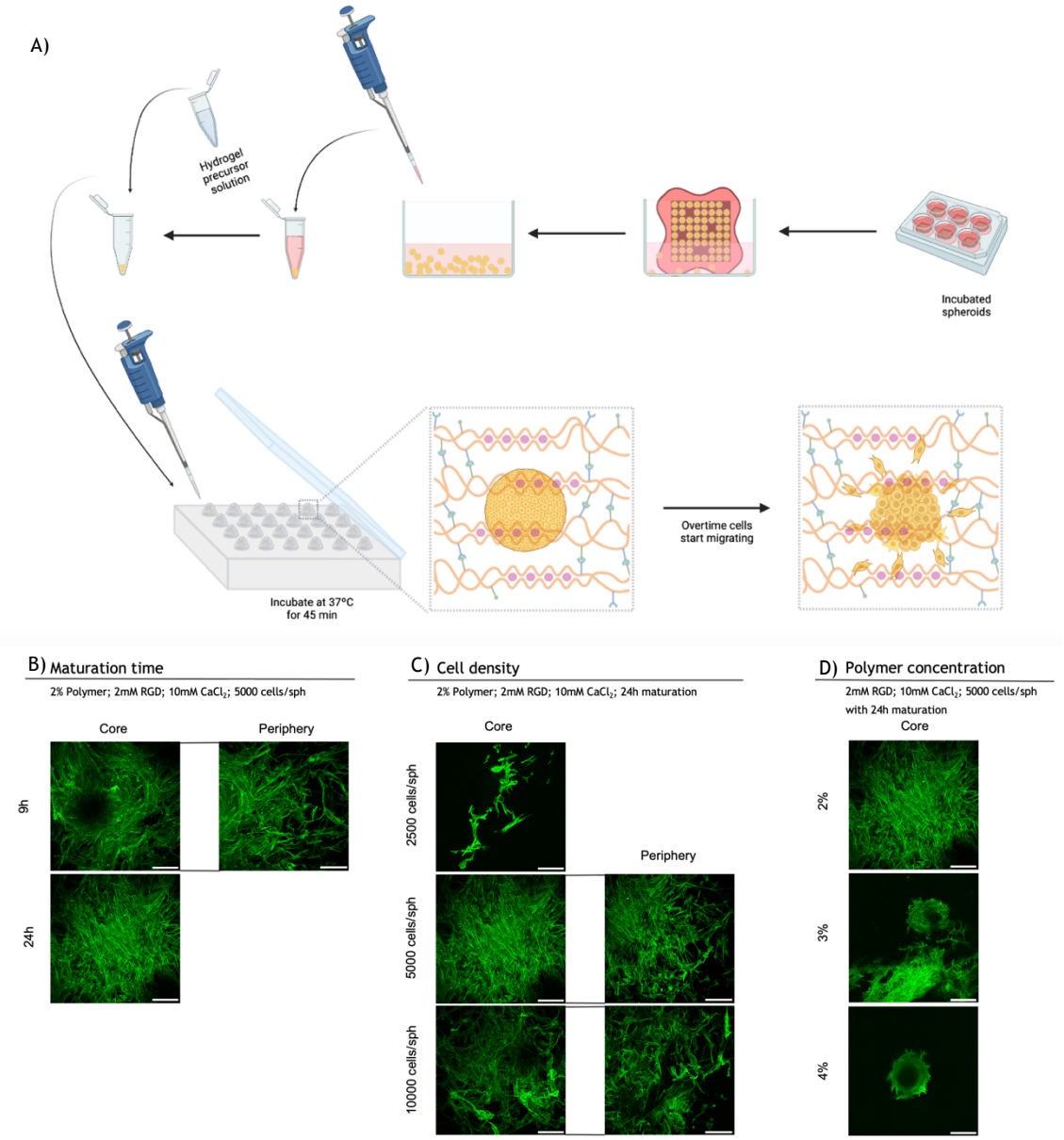

Figure 18 - Schematic illustration of spheroid embedment within the hydrogels (A) and confocal imaging of F-actin staining of fibroblasts after 14 days within the hydrogels with varying polymer concentrations while maintaining RGD at 2mM and $CaCl_2$ at 10mM. (B) Spheroids embedded in 2% polymer hydrogel at different maturation points, 9 and 24 hours after mold seeding. **(C)** Spheroids embedded in hydrogels with different PectX concentrations of 2, 3 and 4%. **(D)** Spheroids embedded in 2% polymer hydrogels with different cell densities, namely 2500, 5000 and 10000 cells per spheroid. The larger images are images of the central zone of the spheroids, while the smaller images are from the periphery to have a better visualization of the sprouting. (Scale bars: 150 µm)

Chapter 5 - Conclusions and Future Work

Severe burns leading to the development of fibrotic tissue, hypertrophic scars, and keloids are a serious socio-economic problem that still exists. Despite existing advances in wound healing and skin regeneration products, these have been below expectations, and there is still no product that truly solves the problem of excessive scar tissue production. Mechanotransduction has been an emerging field of research that has recently been providing seminal contributions to the understanding of how cells as mechanosensitive entities are able to change their biological responses as a function of the biophysical properties of their niche. Thus, herein we propose the development of a biomimetic hydrogel with tunable mechanical properties, in order to study their impact on cellular response in the context of skin repair.

Through the implementation of a dual crosslinking strategy, it was possible to obtain a hydrogel with tunable viscoelastic properties. Furthermore, the incorporation of a cell-adhesive peptide in hydrogels allowed for the addition of relevant biochemical cues that promoted the adhesion of dermal fibroblast cells. Altering the polymer content and the concentration of the ionic crosslinking agent allowed the modulation of the mechanical properties of the hydrogel, namely the elastic and viscous moduli, within the values found in the literature related to healthy skin.

We were able to demonstrate that these hydrogels were highly biocompatible as confocal imaging confirmed high cell viability after 14 days in culture, with almost no detectable dead cells. Furthermore, the modulation of the mechanical and biochemical characteristics of the hydrogels was achieved by varying the concentrations of polymer, $CaCl_2$ and RGD and allowed the observation of changes in the behavior of fibroblasts. It was noticeable that hydrogel does not support cell adhesion without the addition of the cell-adhesive peptide, since the polymer has no cell adhesion sites, and the concentration of RGD for optimal adhesion was determined to be at 2 mM. Changes in calcium concentration allowed the observation that the adhesion and elongation of fibroblasts also increases with the increase of Ca^{2+}, due to the increase in the viscous properties of the hydrogel. However, at some point there was a decline in cells metabolic activity, which could be related to the dynamics of the gel network. Thus, the calcium concentration of 10 mM proved to be ideal, allowing high cell spreading and metabolic activity. Varying the concentration of polymer proved to have a greater impact on the modulation of mechanical properties, which demonstrated to significantly affect cell response. Increasing polymer concentration translated to a decrease of the ability of fibroblasts to elongate as well as to a reduction in their metabolic activity, which were related to the hydrogel's denser and more static network causing confinement to the cells. These results were also validated with the embedding of fibroblasts in these hydrogels at a higher cell density. In softer hydrogels the cells were able to spread homogeneously, and form interconnected

networks with high deposition of fibronectin, while in stiffer gels there was minimal deposition of this ECM component. Finally, the embedding of dermal fibroblast spheroids allowed for the evaluation of cell migration which demonstrated that the mechanical properties of the hydrogels had a great impact. The higher the polymer concentration the greater the difficulty cells had in migrating. Furthermore, maturation time showed no significant differences in this behavior, however lower cell density did show to impact negatively in the formation of the interconnecting cellular networks.

In summary, the developed dual crosslinked hydrogel allowed the modulation of the mechanical and biochemical properties of the hydrogels which were characterized both in terms of mechanical and cellular behavior. Future studies should focus on the detailed characterization of the hydrogel network dynamics (e.g., stress relaxation), sol-gel conversion, and the introduction of cell-degradable sites. In addition, it would be crucial to evaluate in more detail how the mechanical properties of the hydrogels further influence cellular behavior. Thus, it would be beneficial to evaluate the activation of fibroblasts under different conditions, which could be accomplished by immunohistochemical staining of both a-SMA and vimentin as well as through the measurement of TGF-b levels in the medium. Furthermore, it would be relevant to determine the impact of mechanotransduction on the expression of key genes and proteins in the context of healthy and fibrotic tissue formation. Another important factor in skin regeneration and exacerbated scar tissue formation are the signaling pathways that are involved in mechanotransduction. Thus, the pharmacological inhibition of these pathways may allow further evaluation of how the hydrogels are influencing the cell's behavior. A limiting aspect in comparing the hydrogels cultured using with individualized cells and multicellular spheroids was the difference in the number of cells incorporated in each condition. During the spheroid-laden hydrogel formation, it was extremely difficult to guarantee the same number of spheroids per gel by pipetting. Therefore, it would be crucial to develop a method that would allow such control in order to make a more accurate comparison. Lastly, it would also be important to assess if the hydrogel mechanical properties have any impact on the crosstalk between fibroblasts and other important cells involved in the wound healing process.

References

[1] A. Dehdashtian, T. P. Stringer, A. J. Warren, E. W. Mu, B. Amirlak, and L. Shahabi, "Anatomy and Physiology of the Skin," in *Melanoma*, A. I. Riker, Ed. Cham: Springer International Publishing, 2018, pp. 15–26.

[2] A. D. Theocharis, S. S. Skandalis, C. Gialeli, and N. K. Karamanos, "Extracellular matrix structure," *Adv. Drug Deliv. Rev.*, vol. 97, pp. 4–27, 2016, doi: 10.1016/j.addr.2015.11.001.

[3] S. A. Sell, P. S. Wolfe, K. Garg, J. M. McCool, I. A. Rodriguez, and G. L. Bowlin, "The use of natural polymers in tissue engineering: A focus on electrospun extracellular matrix analogues," *Polymers (Basel).*, vol. 2, no. 4, pp. 522–553, 2010, doi: 10.3390/polym2040522.

[4] M. C. Robson, D. L. Steed, and M. G. Franz, "Wound healing: Biologic features and approaches to maximize healing trajectories," *Curr. Probl. Surg.*, vol. 38, no. 2, pp. A1-140, Feb. 2001, doi: 10.1067/msg.2001.111167.

[5] P. Pakshir and B. Hinz, "The big five in fibrosis: Macrophages, myofibroblasts, matrix, mechanics, and miscommunication," *Matrix Biol.*, vol. 68–69, pp. 81–93, 2018, doi: 10.1016/j.matbio.2018.01.019.

[6] T. Wynn, "Cellular and molecular mechanisms of fibrosis," *J. Pathol.*, vol. 214, no. 2, pp. 199–210, Jan. 2008, doi: 10.1002/path.2277.

[7] WHO, "Burns," 2018. https://www.who.int/news-room/fact-sheets/detail/burns (accessed Apr. 19, 2022).

[8] A. B. Association, "Burn Incidence Fact Sheet," *Burn Incidence and Treatment in the United States: 2016*, 2016. https://ameriburn.org/who-we-are/media/burn-incidence-fact-sheet/ (accessed Apr. 29, 2022).

[9] J. F. Guest, G. W. Fuller, and J. Edwards, "Cohort study evaluating management of burns in the community in clinical practice in the UK: Costs and outcomes," *BMJ Open*, vol. 10, no. 4, pp. 1–12, 2020, doi: 10.1136/bmjopen-2019-035345.

[10] T. M. Research, "Burn Injury Treatment Market," 2019. .

[11] I. C. Ng, P. Pawijit, J. Tan, and H. Yu, *Anatomy and physiology for biomaterials research and development*, vol. 1–3. Elsevier, 2019.

[12] M. Norouzi, S. M. Boroujeni, N. Omidvarkordshouli, and M. Soleimani, "Advances in Skin Regeneration: Application of Electrospun Scaffolds," *Adv. Healthc. Mater.*, vol. 4, no. 8, pp. 1114–1133, 2015, doi: 10.1002/adhm.201500001.

[13] D. Sundaramurthi, U. M. Krishnan, and S. Sethuraman, "Electrospun nanofibers as scaffolds for skin tissue engineering," *Polym. Rev.*, vol. 54, no. 2, pp. 348–376, 2014, doi: 10.1080/15583724.2014.881374.

[14] K. Vig *et al.*, "Advances in skin regeneration using tissue engineering," *Int. J. Mol. Sci.*, vol. 18, no. 4, 2017, doi: 10.3390/ijms18040789.

[15] D. Huang *et al.*, "Viscoelasticity in natural tissues and engineered scaffolds for tissue reconstruction," *Acta Biomater.*, vol. 97, pp. 74–92, 2019, doi: 10.1016/j.actbio.2019.08.013.

[16] U. Van Daele *et al.*, "Mechanomodulation: Physical Treatment Modalities Employ Mechanotransduction to Improve Scarring," *Eur. Burn J.*, vol. 3, no. 2, pp. 241–255, 2022, doi: 10.3390/ebj3020021.

[17] A. Dehdashtian, T. P. Stringer, A. J. Warren, E. W. Mu, B. Amirlak, and L. Shahabi, "Anatomy and physiology of the skin," *Melanoma A Mod. Multidiscip. Approach*, pp. 15–26, 2018, doi: 10.1007/978-3-319-78310-9_2.

[18] K. Bohjanen, "Structure and functions of the skin," in *Clinical dermatology*, McGraw-Hill, New York, NY, 2013.

[19] J. M. Abdo, N. A. Sopko, and S. M. Milner, "The applied anatomy of human skin: A model for regeneration," *Wound Med.*, vol. 28, no. December 2019, p. 100179, 2020, doi: 10.1016/j.wndm.2020.100179.

[20] Alice V. Maceo, "Chapter Anatomy and Physiology of Adult Friction," *Fingerpr. Sourceb.*, pp. 2–26, 2011.

[21] J. Khavkin and D. A. F. Ellis, "Aging Skin: Histology, Physiology, and Pathology," *Facial Plast. Surg. Clin. North Am.*, vol. 19, no. 2, pp. 229–234, 2011, doi: 10.1016/j.fsc.2011.04.003.

[22] R. F. Pereira, A. Sousa, C. C. Barrias, A. Bayat, P. L. Granja, and P. J. Bártolo, "Advances in bioprinted cell-laden hydrogels for skin tissue engineering," *Biomanufacturing Rev.*, vol. 2, no. 1, p. 1, Dec. 2017, doi: 10.1007/s40898-017-0003-8.

[23] S. A. Mohamed and R. Hargest, "Surgical anatomy of the skin," *Surg. (United Kingdom)*, vol. 40, no. 1, pp. 1–7, 2022, doi: 10.1016/j.mpsur.2021.11.021.

[24] W. D. Losquadro, "Anatomy of the Skin and the Pathogenesis of Nonmelanoma Skin Cancer," *Facial Plast. Surg. Clin. North Am.*, vol. 25, no. 3, pp. 283–289, 2017, doi: 10.1016/j.fsc.2017.03.001.

[25] M. Venus, J. Waterman, and I. McNab, "Basic physiology of the skin," *Surgery*, vol. 28, no. 10, pp. 469–472, 2010, doi: 10.1016/j.mpsur.2010.07.011.

[26] J. R. Lewis and A. M. Reiter, "Anatomy and physiology," *Small Anim. Dent. Oral Maxillofac. Dis.*, pp. 9–38, 1995, doi: 10.1515/9780691230139-004.

[27] P. A. J. Kolarsick, M. A. Kolarsick, and C. Goodwin, “Anatomy and Physiology of the Skin,” *J. Dermatol. Nurses. Assoc.*, vol. 3, no. 4, pp. 203–213, Jul. 2011, doi: 10.1097/JDN.0b013e3182274a98.

[28] K. Ita, “Anatomy of the human skin,” *Transdermal Drug Deliv.*, pp. 9–18, 2020, doi: 10.1016/b978-0-12-822550-9.00002-8.

[29] S. Lawton, “Skin 1: the structure and functions of the skin,” *Nurs. Times*, vol. 115, no. 12, pp. 30–33, 2019, [Online]. Available: www.nursingtimes.net.

[30] H. P. Gaboriau and C. S. Murakami, “Skin anatomy and flap physiology,” *Otolaryngol. Clin. North Am.*, vol. 34, no. 3, pp. 555–569, 2001, doi: 10.1016/S0030-6665(05)70005-0.

[31] E. Sutterby, P. Thurgood, S. Baratchi, K. Khoshmanesh, and E. Pirogova, “Microfluidic Skin-on-a-Chip Models: Toward Biomimetic Artificial Skin,” *Small*, vol. 16, no. 39, pp. 1–17, 2020, doi: 10.1002/smll.202002515.

[32] R. Mu, S. Campos de Souza, Z. Liao, L. Dong, and C. Wang, “Reprograming the immune niche for skin tissue regeneration – from cellular mechanisms to biomaterials applications,” *Adv. Drug Deliv. Rev.*, vol. 185, p. 114298, 2022, doi: 10.1016/j.addr.2022.114298.

[33] A. L. Rippa, E. P. Kalabusheva, and E. A. Vorotelyak, “Regeneration of Dermis: Scarring and Cells Involved,” *Cells*, vol. 8, no. 6, p. 607, 2019, doi: 10.3390/cells8060607.

[34] S. S. Kordestani, “Wound Anatomy,” *Atlas Wound Heal.*, pp. 3–9, 2019, doi: 10.1016/b978-0-323-67968-8.00002-1.

[35] G. S. Schultz and A. Wysocki, “Interactions between extracellular matrix and growth factors in wound healing,” *Wound Repair Regen.*, vol. 17, no. 2, pp. 153–162, 2009, doi: 10.1111/j.1524-475X.2009.00466.x.

[36] S. H. Kim, J. Turnbull, and S. Guimond, “Extracellular matrix and cell signalling: The dynamic cooperation of integrin, proteoglycan and growth factor receptor,” *J. Endocrinol.*, vol. 209, no. 2, pp. 139–151, 2011, doi: 10.1530/JOE-10-0377.

[37] S. A. Hoda and E. Cheng, “Robbins Basic Pathology,” *Am. J. Clin. Pathol.*, vol. 148, no. 6, pp. 557–557, Nov. 2017, doi: 10.1093/ajcp/aqx095.

[38] G. Huang *et al.*, “Functional and Biomimetic Materials for Engineering of the Three-Dimensional Cell Microenvironment,” *Chem. Rev.*, vol. 117, no. 20, pp. 12764–12850, 2017, doi: 10.1021/acs.chemrev.7b00094.

[39] T. Nemoto, R. Kubota, Y. Murasawa, and Z. Isogai, “Viscoelastic Properties of the Human Dermis and Other Connective Tissues and Its Relevance to Tissue Aging and Aging-Related Disease,” in *Viscoelasticity - From Theory to Biological Applications*, InTech, 2012, p. 13.

[40] K. C. Clause and T. H. Barker, “Extracellular matrix signaling in morphogenesis and repair,” *Curr. Opin. Biotechnol.*, vol. 24, no. 5, pp. 830–833, 2013, doi: 10.1016/j.copbio.2013.04.011.

[41] C. P. Barnes, S. A. Sell, E. D. Boland, D. G. Simpson, and G. L. Bowlin, “Nanofiber technology: Designing the next generation of tissue engineering scaffolds,” *Adv. Drug Deliv. Rev.*, vol. 59, no. 14, pp. 1413–1433, 2007, doi: 10.1016/j.addr.2007.04.022.

[42] M. Petreaca and M. Martins-Green, *The Dynamics of Cell-ECM Interactions, with Implications for Tissue Engineering*, Fourth Edi. Elsevier, 2013.

[43] T. Rozario and D. W. DeSimone, “The extracellular matrix in development and morphogenesis: A dynamic view,” *Dev. Biol.*, vol. 341, no. 1, pp. 126–140, 2010, doi: 10.1016/j.ydbio.2009.10.026.

[44] N. K. Rajendran, S. S. D. Kumar, N. N. Houreld, and H. Abrahamse, “A review on nanoparticle based treatment for wound healing,” *J. Drug Deliv. Sci. Technol.*, vol. 44, no. January, pp. 421–430, 2018, doi: 10.1016/j.jddst.2018.01.009.

[45] S. R. Goldberg and R. F. Diegelmann, “Wound Healing Primer,” *Surg. Clin. North Am.*, vol. 90, no. 6, pp. 1133–1146, 2010, doi: 10.1016/j.suc.2010.08.003.

[46] S. Enoch and P. Price, “Cellular, molecular and biochemical differences in the pathophysiology of healing between acute wounds, chronic wounds and wounds in the aged,” *World Wide Wounds*, vol. 2005, no. August, 2004.

[47] T. Velnar, T. Bailey, and V. Smrkolj, “The wound healing process: An overview of the cellular and molecular mechanisms,” *J. Int. Med. Res.*, vol. 37, no. 5, pp. 1528–1542, 2009, doi: 10.1177/147323000903700531.

[48] G. Broughton, J. E. Janis, and C. E. Attinger, “Wound healing: An overview,” *Plast. Reconstr. Surg.*, vol. 117, no. 7 SUPPL., pp. 1–32, 2006, doi: 10.1097/01.prs.0000222562.60260.f9.

[49] S. S. Ramasastry, “Acute wounds,” *Clin. Plast. Surg.*, vol. 32, no. 2, pp. 195–208, 2005, doi: 10.1016/j.cps.2004.12.001.

[50] S. Singh, A. Young, and C. E. McNaught, “The physiology of wound healing,” *Surg. (United Kingdom)*, vol. 35, no. 9, pp. 473–477, 2017, doi: 10.1016/j.mpsur.2017.06.004.

[51] F. Strodtbeck, “Physiology of wound healing,” *Newborn Infant Nurs. Rev.*, vol. 1, no. 1, pp. 43–52, 2001, doi: 10.1053/nbin.2001.23176.

[52] T. O. H. Prasetyono, “General concept of wound healing, revisited,” *Med. J. Indones.*, vol. 18, no. 3, pp. 208–216, 2009, doi: 10.13181/mji.v18i3.364.

[53] A. C. D. O. Gonzalez, Z. D. A. Andrade, T. F. Costa, and A. R. A. P. Medrado, “Wound healing - A literature review,” *An. Bras. Dermatol.*, vol. 91, no. 5, pp. 614–620, 2016, doi: 10.1590/abd1806-4841.20164741.

[54] E. A. Gantwerker and D. B. Hom, “Skin: Histology and physiology of wound healing,” *Clin. Plast. Surg.*, vol. 39, no. 1, pp. 85–97, 2012, doi: 10.1016/j.cps.2011.09.005.

[55] F. Thiruvoth, D. Mohapatra, D. Sivakumar, R. Chittoria, and V. Nandhagopal, “Current concepts in the physiology of adult wound healing,” *Plast. Aesthetic Res.*, vol. 2, no. 5, p. 250, 2015, doi: 10.4103/2347-9264.158851.

[56] S. Sanon, D. A. Hart, and E. E. Tredget, *Molecular and Cellular Biology of Wound Healing and Skin Regeneration*. Elsevier Inc., 2016.

[57] S. S. Kordestani, “Burn Wounds,” *Atlas Wound Heal.*, pp. 101–114, 2019, doi: 10.1016/b978-0-323-67968-8.00009-4.

[58] A. El Ayadi, J. W. Jay, and A. Prasai, “Current approaches targeting the wound healing phases to attenuate fibrosis and scarring,” *Int. J. Mol. Sci.*, vol. 21, no. 3, 2020, doi: 10.3390/ijms21031105.

[59] Y. Wang *et al.*, “Burn injury: Challenges and advances in burn wound healing, infection, pain and scarring,” *Adv. Drug Deliv. Rev.*, vol. 123, pp. 3–17, 2018, doi: 10.1016/j.addr.2017.09.018.

[60] E. G. Brownson and N. S. Gibran, *Evaluation of the burn wound: Management decisions*, Fifth Edit. Elsevier Inc., 2018.

[61] K. Osborn, *Burn wound management*. Elsevier Inc., 2018.

[62] G. P. Sidgwick, D. McGeorge, and A. Bayat, “A comprehensive evidence-based review on the role of topicals and dressings in the management of skin scarring,” *Arch. Dermatol. Res.*, vol. 307, no. 6, pp. 461–477, Aug. 2015, doi: 10.1007/s00403-015-1572-0.

[63] G. G. Gauglitz, H. C. Korting, T. Pavicic, T. Ruzicka, and M. G. Jeschke, “Hypertrophic scarring and keloids: Pathomechanisms and current and emerging treatment strategies,” *Mol. Med.*, vol. 17, no. 1–2, pp. 113–125, 2011, doi: 10.2119/molmed.2009.00153.

[64] P. A. Sundaram, *Mechanotransduction Cell Signaling to Cell Response*, vol. 7, no. 1. ACADEMIC PRESS, 2021.

[65] B. Kuehlmann, C. A. Bonham, I. Zucal, L. Prantl, and G. C. Gurtner, “Mechanotransduction in wound healing and fibrosis,” *J. Clin. Med.*, vol. 9, no. 5, pp. 1–19, 2020, doi: 10.3390/jcm9051423.

[66] F. G. Becker *et al.*, *Molecular Mechanisms od Skin Aging and Age-Related Diseases*, vol. 7, no. 1. 2015.

[67] S. Fu *et al.*, “Mechanotransduction in wound healing: From the cellular and molecular level to the clinic,” *Adv. Ski. Wound Care*, vol. 34, no. 2, pp. 67–74, 2021, doi: 10.1097/01.ASW.0000725220.92976.a7.

[68] O. Chaudhuri, J. Cooper-White, P. A. Janmey, D. J. Mooney, and V. B. Shenoy, “Effects of extracellular matrix viscoelasticity on cellular behaviour,” *Nature*, vol. 584, no. 7822, pp. 535–546, 2020, doi: 10.1038/s41586-020-2612-2.

[69] S. H. Hussain, B. Limthongkul, and T. R. Humphreys, “The Biomechanical Properties of the Skin,” *Dermatologic Surg.*, vol. 39, no. 2, pp. 193–203, 2013, doi: 10.1111/dsu.12095.

[70] K. Zhang, Q. Feng, Z. Fang, L. Gu, and L. Bian, “Structurally Dynamic Hydrogels for Biomedical Applications: Pursuing a Fine Balance between Macroscopic Stability and Microscopic Dynamics,” *Chem. Rev.*, vol. 121, no. 18, pp. 11149–11193, 2021, doi: 10.1021/acs.chemrev.1c00071.

[71] D. T. Corr and D. A. Hart, “Biomechanics of Scar Tissue and Uninjured Skin,” *Adv. Wound Care*, vol. 2, no. 2, pp. 37–43, 2013, doi: 10.1089/wound.2011.0321.

[72] D. T. Corr and D. A. Hart, “Biomechanics of Scar Tissue and Uninjured Skin,” *Adv. Wound Care*, vol. 2, no. 2, pp. 37–43, Mar. 2013, doi: 10.1089/wound.2011.0321.

[73] G. A. Martău, M. Mihai, and D. C. Vodnar, “The Use of Chitosan, Alginate, and Pectin in the Biomedical and Food Sector—Biocompatibility, Bioadhesiveness, and Biodegradability,” *Polymers (Basel).*, vol. 11, no. 11, p. 1837, Nov. 2019, doi: 10.3390/polym11111837.

[74] M. Gomez-Florit *et al.*, “Natural-Based Hydrogels for Tissue Engineering Applications,” *Molecules*, vol. 25, no. 24, pp. 1–29, 2020, doi: 10.3390/molecules25245858.

[75] T. Chhibber *et al.*, “Hydrogels in Tissue Engineering,” *Intell. Hydrogels Diagnostics Ther.*, no. May, pp. 105–122, 2020, doi: 10.1201/9781003036050-8.

[76] S. Bashir *et al.*, “Fundamental Concepts of Hydrogels: Synthesis, Properties, and Their Applications,” *Polymers (Basel).*, vol. 12, no. 11, p. 2702, Nov. 2020, doi: 10.3390/polym12112702.

[77] I. Firlar, M. Altunbek, C. McCarthy, M. Ramalingam, and G. Camci-Unal, “Functional Hydrogels for Treatment of Chronic Wounds,” *Gels*, vol. 8, no. 2, pp. 1–23, 2022, doi: 10.3390/gels8020127.

[78] S. Cascone and G. Lamberti, “Hydrogel-based commercial products for biomedical applications: A review,” *Int. J. Pharm.*, vol. 573, no. October 2019, p. 118803, 2020, doi: 10.1016/j.ijpharm.2019.118803.

[79] C. M. P. Freitas, J. S. R. Coimbra, V. G. L. Souza, and R. C. S. Sousa, “Structure and Applications of Pectin in Food, Biomedical, and Pharmaceutical Industry: A Review,” *Coatings*, vol. 11, no. 8, p. 922, Aug. 2021, doi: 10.3390/coatings11080922.

[80] I. Gholamali, “Stimuli-Responsive Polysaccharide Hydrogels for Biomedical Applications: a Review,” *Regen. Eng. Transl. Med.*, vol. 7, no. 1, pp. 91–114, 2021, doi: 10.1007/s40883-019-00134-1.

[81] A. Zdunek, P. M. Pieczywek, and J. Cybulska, “The primary, secondary, and structures of higher levels of pectin polysaccharides,” *Compr. Rev. Food Sci. Food Saf.*, vol. 20, no. 1, pp. 1101–1117, Jan. 2021, doi: 10.1111/1541-4337.12689.

[82] D. qiang Li *et al.*, “Pectin in biomedical and drug delivery applications: A review,” *Int. J. Biol. Macromol.*, vol. 185, no. June, pp. 49–65, 2021, doi: 10.1016/j.ijbiomac.2021.06.088.

[83] M. C. N. Picot-Allain, B. Ramasawmy, and M. N. Emmambux, “Extraction, Characterisation, and Application of Pectin from Tropical and Sub-Tropical Fruits: A Review,” *Food Rev. Int.*, vol. 38, no. 3, pp. 282–312, 2022, doi: 10.1080/87559129.2020.1733008.

[84] G. A. Martau, M. Mihai, and D. C. Vodnar, “The use of chitosan, alginate, and pectin in the biomedical and food sector-biocompatibility, bioadhesiveness, and biodegradability,” *Polymers (Basel).*, vol. 11, no. 11, 2019, doi: 10.3390/polym11111837.

[85] R. F. Pereira, “Bioprinting of cell-responsive bioinks for skin tissue engineering,” Instituto de Ciências Biomédicas Abel Salazar, 2018.

[86] M. Sadeghi, “Pectin-Based Biodegradable Hydrogels with Potential Biomedical Applications as Drug Delivery Systems,” *J. Biomater. Nanobiotechnol.*, vol. 02, no. 01, pp. 36–40, 2011, doi: 10.4236/jbnb.2011.21005.

[87] D. qiang Li *et al.*, “Pectin in biomedical and drug delivery applications: A review,” *Int. J. Biol. Macromol.*, vol. 185, no. March, pp. 49–65, 2021, doi: 10.1016/j.ijbiomac.2021.06.088.

[88] J. Lou, R. Stowers, S. Nam, Y. Xia, and O. Chaudhuri, “Stress relaxing hyaluronic acid-collagen hydrogels promote cell spreading, fiber remodeling, and focal adhesion formation in 3D cell culture,” *Biomaterials*, vol. 154, pp. 213–222, Feb. 2018, doi: 10.1016/j.biomaterials.2017.11.004.

[89] M. Rizwan, A. E. G. Baker, and M. S. Shoichet, “Designing Hydrogels for 3D Cell Culture Using Dynamic Covalent Crosslinking,” *Adv. Healthc. Mater.*, vol. 10, no. 12, pp. 1–23, 2021, doi: 10.1002/adhm.202100234.

[90] Y. Ma *et al.*, “Viscoelastic Cell Microenvironment: Hydrogel-Based Strategy for Recapitulating Dynamic ECM Mechanics,” *Adv. Funct. Mater.*, vol. 31, no. 24, pp. 1–26, 2021, doi: 10.1002/adfm.202100848.

[91] N. Reddy, R. Reddy, and Q. Jiang, “Crosslinking biopolymers for biomedical applications,” *Trends Biotechnol.*, vol. 33, no. 6, pp. 362–369, 2015, doi: 10.1016/j.tibtech.2015.03.008.

[92] A. GhavamiNejad, N. Ashammakhi, X. Y. Wu, and A. Khademhosseini, “Crosslinking Strategies for 3D Bioprinting of Polymeric Hydrogels,” *Small*, vol. 16, no. 35, pp. 1–30, 2020, doi: 10.1002/smll.202002931.

[93] W. Hu, Z. Wang, Y. Xiao, S. Zhang, and J. Wang, “Advances in crosslinking strategies of biomedical hydrogels,” *Biomater. Sci.*, vol. 7, no. 3, pp. 843–855, 2019, doi: 10.1039/c8bm01246f.

[94] Y. Zhou, S. P. Petrova, and K. J. Edgar, “Chemical synthesis of polysaccharide–protein and polysaccharide–peptide conjugates: A review,” *Carbohydr. Polym.*, vol. 274, no. September, p. 118662, 2021, doi: 10.1016/j.carbpol.2021.118662.

[95] J. Xiang, L. Shen, and Y. Hong, “Status and future scope of hydrogels in wound healing: Synthesis, materials and evaluation,” *Eur. Polym. J.*, vol. 130, no. February, p. 109609, 2020, doi: 10.1016/j.eurpolymj.2020.109609.

[96] W. Wang, R. Narain, and H. Zeng, *Hydrogels*. Elsevier Inc., 2020.

[97] J. Maitra and V. K. Shukla, “Cross-linking in Hydrogels - A Review,” *Am. J. Polym. Sci.*, vol. 4, no. 2, pp. 25–31, 2014, doi: 10.5923/j.ajps.20140402.01.

[98] H. Nosrati, M. Khodaei, Z. Alizadeh, and M. Banitalebi-Dehkordi, “Cationic, anionic and neutral polysaccharides for skin tissue engineering and wound healing applications,” *Int. J. Biol. Macromol.*, vol. 192, no. July, pp. 298–322, 2021, doi: 10.1016/j.ijbiomac.2021.10.013.

[99] L. Cao, W. Lu, A. Mata, K. Nishinari, and Y. Fang, “Egg-box model-based gelation of alginate and pectin: A review,” *Carbohydr. Polym.*, vol. 242, no. January, p. 116389, 2020, doi: 10.1016/j.carbpol.2020.116389.

[100] L. Aguero, S. Alpdagtas, E. Ilhan, D. Zaldivar-Silva, and O. Gunduz, “Functional role of crosslinking in alginate scaffold for drug delivery and tissue engineering: A review,” *Eur. Polym. J.*, vol. 160, p. 110807, Nov. 2021, doi: 10.1016/j.eurpolymj.2021.110807.

[101] C. Hu, W. Lu, A. Mata, K. Nishinari, and Y. Fang, “Ions-induced gelation of alginate: Mechanisms and applications,” *Int. J. Biol. Macromol.*, vol. 177, pp. 578–588, Apr. 2021, doi: 10.1016/j.ijbiomac.2021.02.086.

[102] T. N. Gevrek and A. Sanyal, “Furan-containing polymeric Materials: Harnessing the Diels-Alder chemistry for biomedical applications,” *Eur. Polym. J.*, vol. 153, no. May, p. 110514, 2021, doi: 10.1016/j.eurpolymj.2021.110514.

[103] E. Hui, J. L. Sumey, and S. R. Caliari, “Click-functionalized hydrogel design for mechanobiology investigations,” *Mol. Syst. Des. Eng.*, vol. 6, no. 9, pp. 670–707, 2021, doi: 10.1039/D1ME00049G.

[104] M. R. Arkenberg, H. D. Nguyen, and C. C. Lin, “Recent advances in bio-orthogonal and dynamic crosslinking of biomimetic hydrogels,” *J. Mater. Chem. B*, vol. 8, no. 35, pp. 7835–7855, 2020, doi: 10.1039/d0tb01429j.

[105] V. G. Muir and J. A. Burdick, “Chemically Modified Biopolymers for the Formation of Biomedical Hydrogels,” *Chem. Rev.*, vol. 121, no. 18, pp. 10908–10949, 2021, doi: 10.1021/acs.chemrev.0c00923.

[106] M. I. L. Soares, A. L. Cardoso, and T. M. V. D. Pinho e Melo, “Diels–Alder Cycloaddition Reactions in Sustainable Media,” *Molecules*, vol. 27, no. 4, p. 1304, Feb. 2022, doi: 10.3390/molecules27041304.

[107] M. G. Fernandes *et al.*, “Mechanomodulatory Biomaterials Prospects in Scar Prevention and Treatment.,” *Acta Biomater.*, no. xxxx, 2022, doi: 10.1016/j.actbio.2022.07.042.

[108] C. Branco da Cunha *et al.*, “Influence of the stiffness of three-dimensional alginate/collagen-I interpenetrating networks on fibroblast biology,” *Biomaterials*, vol. 35, no. 32, pp. 8927–8936, Oct. 2014, doi: 10.1016/j.biomaterials.2014.06.047.

[109] S. Nam, R. Stowers, J. Lou, Y. Xia, and O. Chaudhuri, “Varying PEG density to control stress relaxation in alginate-PEG hydrogels for 3D cell culture studies,” *Biomaterials*, vol. 200, pp. 15–24, Apr. 2019, doi: 10.1016/j.biomaterials.2019.02.004.

[110] J. Hazur, N. Endrizzi, D. W. Schubert, A. R. Boccaccini, and B. Fabry, “Stress relaxation amplitude of hydrogels determines migration, proliferation, and morphology of cells in 3-D culture,” *Biomater. Sci.*, vol. 10, no. 1, pp. 270–280, 2022, doi: 10.1039/D1BM01089A.

[111] S. Mahadevaiah, K. G. Robinson, P. M. Kharkar, K. L. Kiick, and R. E. Akins, “Decreasing matrix modulus of PEG hydrogels induces a vascular phenotype in human cord blood stem cells,” *Biomaterials*, vol. 62, pp. 24–34, Sep. 2015, doi: 10.1016/j.biomaterials.2015.05.021.

[112] B. J. Carberry, V. V. Rao, and K. S. Anseth, “Phototunable Viscoelasticity in Hydrogels Through Thioester Exchange,” *Ann. Biomed. Eng.*, vol. 48, no. 7, pp. 2053–2063, Jul. 2020, doi: 10.1007/s10439-020-02460-w.

[113] M.-Y. Shie, J.-J. Lee, C.-C. Ho, S.-Y. Yen, H. Y. Ng, and Y.-W. Chen, “Effects of Gelatin Methacrylate Bio-ink Concentration on Mechano-Physical Properties and Human Dermal Fibroblast Behavior,” *Polymers (Basel).*, vol. 12, no. 9, p. 1930, Aug. 2020, doi: 10.3390/polym12091930.

[114] R. F. Pereira, A. Sousa, C. C. Barrias, P. J. Bártolo, and P. L. Granja, “A single-component hydrogel bioink for bioprinting of bioengineered 3D constructs for dermal tissue engineering,” *Mater. Horizons*, vol. 5, no. 6, pp. 1100–1111, 2018, doi: 10.1039/C8MH00525G.

[115] C. M. Nimmo, S. C. Owen, and M. S. Shoichet, “Diels−Alder Click Cross-Linked Hyaluronic Acid Hydrogels for Tissue Engineering,” *Biomacromolecules*, vol. 12, no. 3, pp. 824–830, Mar. 2011, doi: 10.1021/bm101446k.

[116] S. J. Bidarra, C. C. Barrias, K. B. Fonseca, M. A. Barbosa, R. A. Soares, and P. L. Granja, “Injectable in situ crosslinkable RGD-modified alginate matrix for endothelial cells delivery,” *Biomaterials*, vol. 32, no. 31, pp. 7897–7904, Nov. 2011, doi: 10.1016/j.biomaterials.2011.07.013.

[117] B. D. Plouffe, M. A. Brown, R. K. Iyer, M. Radisic, and S. K. Murthy, “Controlled capture and release of cardiac fibroblasts using peptide-functionalized alginate gels in microfluidic channels,” *Lab Chip*, vol. 9, no. 11, p. 1507, 2009, doi: 10.1039/b823523f.

[118] Z. Deng, F. Liu, and C. Li, “Therapeutic effect of ethylenediaminetetraacetic acid irrigation solution against wound infection with drug-resistant bacteria in a rat model: an animal study,” *Bone Joint Res.*, vol. 8, no. 5, pp. 189–198, May 2019, doi: 10.1302/2046-3758.85.BJR-2018-0280.R3.

[119] C. K. Hsu, H. H. Lin, H. I. C. Harn, M. W. Hughes, M. J. Tang, and C. C. Yang, “Mechanical forces in skin disorders,” *J. Dermatol. Sci.*, vol. 90, no. 3, pp. 232–240, 2018, doi: 10.1016/j.jdermsci.2018.03.004.

[120] R. F. Pereira, C. C. Barrias, P. J. Bártolo, and P. L. Granja, “Cell-instructive pectin hydrogels crosslinked via thiol-norbornene photo-click chemistry for skin tissue engineering,” *Acta Biomater.*, vol. 66, pp. 282–293, 2018, doi: 10.1016/j.actbio.2017.11.016.

[121] J. Patten and K. Wang, “Fibronectin in development and wound healing,” *Adv. Drug Deliv. Rev.*, vol. 170, pp. 353–368, Mar. 2021, doi: 10.1016/j.addr.2020.09.005.

[122] Y. Lee, J. W. Bae, J. W. Lee, W. Suh, and K. D. Park, “Enzyme-catalyzed in situ forming gelatin hydrogels as bioactive wound dressings: effects of fibroblast delivery on wound healing efficacy,” *J. Mater. Chem. B*, vol. 2, no. 44, pp. 7712–7718, 2014, doi: 10.1039/C4TB01111B.

[123] S. Kim, E. M. Kim, M. Yamamoto, H. Park, and H. Shin, “Engineering Multi-Cellular Spheroids for Tissue Engineering and Regenerative Medicine,” *Adv. Healthc. Mater.*, vol. 9, no. 23, p. 2000608, Dec. 2020, doi: 10.1002/adhm.202000608.

[124] Y. Tan, A. Suarez, M. Garza, A. A. Khan, J. Elisseeff, and D. Coon, “Human fibroblast-macrophage tissue spheroids demonstrate ratio-dependent fibrotic activity for in vitro fibrogenesis model development,” *Biomater. Sci.*, vol. 8, no. 7, pp. 1951–1960, 2020, doi: 10.1039/C9BM00900K.

[125] E. M. Kim *et al.*, “Effects of mechanical properties of gelatin methacryloyl hydrogels on encapsulated stem cell spheroids for 3D tissue engineering,” *Int. J. Biol. Macromol.*, vol. 194, pp. 903–913, Jan. 2022, doi: 10.1016/j.ijbiomac.2021.11.145.

Supplementary Data

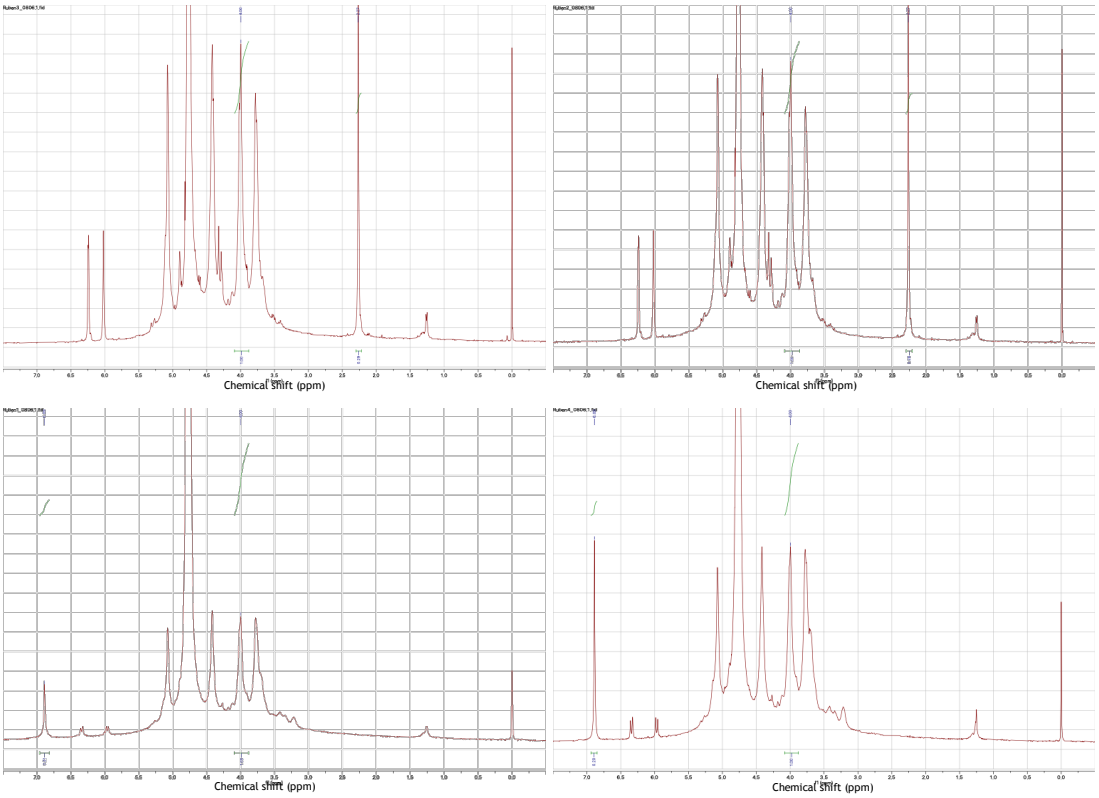

Figure S1 - ^{1}H NMR spectra (D2O, 400MHz) of two separate PectX-FUR (A), and PectX-MAL (B) functionalization, demonstrating reproducibility through similar integrals of their peaks.

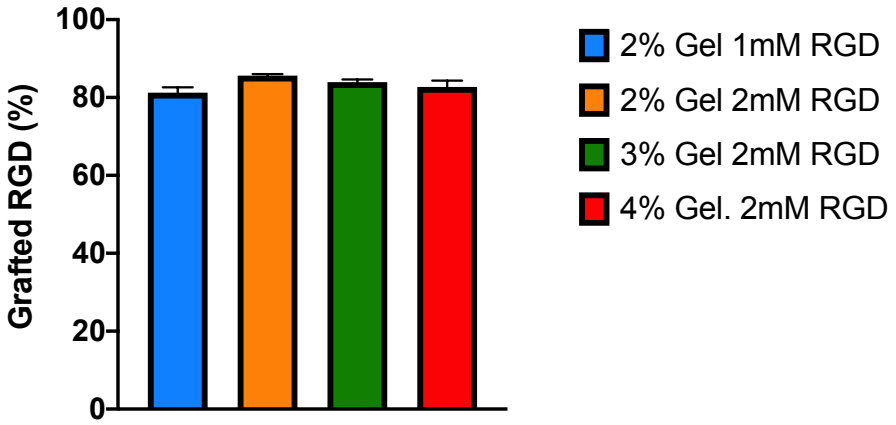

Figure S2 - Percentage of grafted RGD into the hydrogels, comparing the use of different concentrations of both the peptide and the polymer. The assay was performed by fluorescence quantification of untethered peptide (CGGGGRGDSP-FITC) upon 24h incubation in HBSS.